Naval Research Laboratory

Washington, DC 20375-5320

NRL/MR/5320--10-9232

Experiments in Weight Design for a Sombrero Array Pattern

KELLY R. MCPHAIL
JEFFREY O. COLEMAN
DAN P. SCHOLNIK

Advanced Radar Systems Branch
Radar Division

June 25, 2010

REPORT DOCUMENTATION PAGE

Form Approved
OMB No. 0704-0188

1. REPORT DATE *(DD-MM-YYYY)*	**2. REPORT TYPE**	**3. DATES COVERED** *(From - To)*
25-06-2010	Memorandum Report	

4. TITLE AND SUBTITLE

Experiments in Weight Design for a Sombrero Array Pattern

5a. CONTRACT NUMBER

5b. GRANT NUMBER

5c. PROGRAM ELEMENT NUMBER
61153N

6. AUTHOR(S)

Kelly R. McPhail, Jeffrey O. Coleman, and Dan P. Scholnik

5d. PROJECT NUMBER

5e. TASK NUMBER

5f. WORK UNIT NUMBER
9895

7. PERFORMING ORGANIZATION NAME(S) AND ADDRESS(ES)

Naval Research Laboratory
4555 Overlook Avenue, SW
Washington, DC 20375-5320

8. PERFORMING ORGANIZATION REPORT NUMBER

NRL/MR/5320--10-9232

9. SPONSORING / MONITORING AGENCY NAME(S) AND ADDRESS(ES)

Naval Research Laboratory
4555 Overlook Avenue, SW
Washington, DC 20375-5320

10. SPONSOR / MONITOR'S ACRONYM(S)
NRL

11. SPONSOR / MONITOR'S REPORT NUMBER(S)

12. DISTRIBUTION / AVAILABILITY STATEMENT

Approved for public release; distribution is unlimited.

13. SUPPLEMENTARY NOTES

14. ABSTRACT

There is an interest in developing a transmit array taper that illuminates both a highly directive cluster of receive beams and a broad region of the sky at a level that can support a ubiquitous radar function. This report provides experimental optimization results of a sombrero-shaped amplitude array taper that can be used to implement two simultaneous functions of this type. The amplitude tapers are optimized in two ways: boresight radiated power density is fixed while minimizing either max total transmitter power required or max element power required. This report also presents experiments with nonoptimized linear-FM and nonlinear-FM phase-only tapers. The phase-only tapers do improve the peak level loss that occurs in the amplitude optimizations. We do not have the capability to optimize phase-only weights, but intend to give a designer a starting point for exploring phase-only optimization of a sombrero-shaped array factor.

15. SUBJECT TERMS
Array pattern
Amplitude taper
Phase-only taper
Optimization
Second-order cone programming

16. SECURITY CLASSIFICATION OF:			**17. LIMITATION OF ABSTRACT**	**18. NUMBER OF PAGES**	**19a. NAME OF RESPONSIBLE PERSON**
a. REPORT	**b. ABSTRACT**	**c. THIS PAGE**			Dan P. Scholnik
Unclassified	Unclassified	Unclassified	UL	71	**19b. TELEPHONE NUMBER** *(include area code)* (202) 404-1943

Standard Form 298 (Rev. 8-98)
Prescribed by ANSI Std. Z39.18

Contents

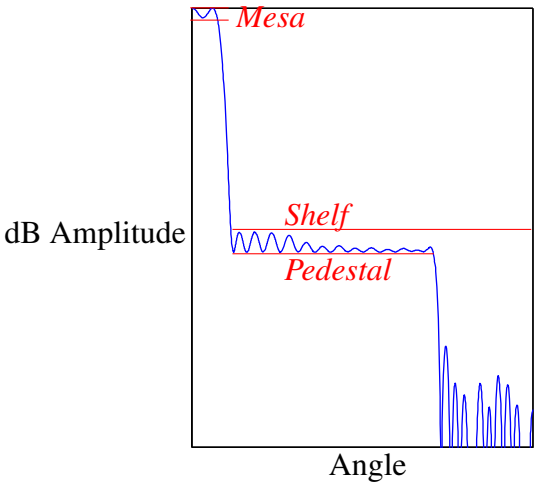

Figure 1: *Mesa*, *Shelf* and *Pedestal* constraints are chosen to optimize an array factor with this sombrero shape.

1 Introduction

Suppose we have a planar transmit array of weighted antenna elements laid out on a lattice, a regular grid, and suppose each embedded element pattern is identical (typically achieved using guard elements). Then the far-field array pattern is just the product of the embedded element pattern and an array factor that is the 2D Fourier transform of the array taper. Mathematically, the array taper comprises impulses at the element locations with areas given by the element weights. We can speak of designing the weights, the taper, or the array factor. These are equivalent.

Is it possible to optimize a transmit array taper that illuminates both a highly directive cluster of receive beams and a broad region of the sky, perhaps to support a ubiquitous radar function [1, 2]? Such a transmit array factor might allow us to track several targets and simultaneously monitor a broad region of interest for new targets. The goal of this report is to determine whether it is feasible to design a transmit array taper with such characteristics. The larger issues involved in designing such a radar system are outside the scope of this report and will not be addressed.

The array factor that we desire has what we call a sombrero structure (Figure 1), where the term *mesa* refers to the top of the sombrero, *shelf* refers to the top of the sombrero's brim and *pedestal* refers to the bottom of the sombrero's brim. The optimized amplitude-taper designs that follow have constraints in one or more of the angle regions defined by these terms. Constraints on the mesa region limit passband ripple, constraints on the shelf region limit the array-factor magnitude in the stopband, and constraints on the pedestal region define the height of the sombrero's brim.

In this report we are particularly interested in an "active" transmit array, in which each element is driven by its own power amplifier. There are two basic categories. In one category, the power radiated is limited by the power available from individual elements. The output-power capabilities of the individual amplifiers driving the elements is the determining factor. In the other category, the power radiated is limited only by a constraint on total transmit power as determined by available prime power or by heat-dissipation issues, and individual amplifiers can provide power as needed. These two categories are idealizations;

Manuscript approved April 16, 2010.

in real systems power might well be constrained by both a total-power limit and by per-element power. However, consideration of these two extremes reveals a key choice: given a desired target illumination level, should our weight design minimize peak element power or total transmit power?

Minimizing peak element power (without other design constraints) leads naturally to a phase-only taper. All element weights have the same magnitude. To minimize total transmit power, however, complex weights are needed, and design symmetries typically lead to weight phases being used only for beam steering so that the unsteered taper is a pure amplitude taper.

Amplitude tapers are our main focus, not because they are what is most needed or desired but simply because we have first-rate tools for designing complex or amplitude tapers but are limited to the crudest of design methods for phase-only tapers. That situation is not entirely about software and methods but is about the problem itself: a phase is one degree of freedom, but a complex weight is two. Should we not expect that doubling the number of degrees of freedom will permit better optimization? Further and more important is that the two design spaces are different in a fundamental geometric sense. The amplitude-taper space is smoothly shaped and easily searched, while the phase-only space is jagged and rough, a problem only made incomprehensibly worse by the high dimensionality—often thousands—of the space. It's largely unsearchable except by trial and error.

So here we explore complex or amplitude tapers at some length and phase-only tapers quite tentatively. Phase-only tapers are a subset of complex tapers of course, so if there is no good solution to the complex-taper sombrero design problem, there cannot be a good solution to the phase-only sombrero problem either. Addressing complex tapers first then implicitly seeks to learn whether there is something in the nature of array factors themselves that precludes a sombrero structure. If our answer had been "no sombreros allowed", it would have applied to both types of tapers. As it turns out, that is not our answer.

Certain details are common to every design presented in this report. All of the designs in this report assume a roughly circular 4507 element array arranged on a $\lambda/\sqrt{3}$ spaced equilateral triangular grid (Figure 2). For ease of optimization, we require that the taper be unchanged when the whole array is subjected to any of the five indicated rotations or mirrored through any of the six lines shown in Figure 3. This automatically makes the array factor invariant to those same rotations and reflections. These array symmetries reduce the number of optimization variables by a factor of roughly 12. A real design might well call for a nonsymmetric pattern, but this approach provides the essential insight into the trade space at a much reduced computational cost. We assume a narrowband array and do not consider the wideband case. In each design we show boresight beams, however it is possible to phase steer any of these array factors off of boresight.

Section 2 presents optimized amplitude taper designs. These amplitude taper designs start with a very simple pencil beam design and work towards the sombrero pattern described above. The report includes a progression of designs to show the effects of each constraint that is added to the optimization to eventually produce the sombrero pattern.

Section 3 presents several phase-only tapers constructed as 2D chirps, with linear-chirp designs followed by nonlinear-chirp designs. Chirp parameters were chosen and tweaked by hand, simply by trial and error. The results are rough and serve mostly to illustrate the severity of the phase-only limitation.

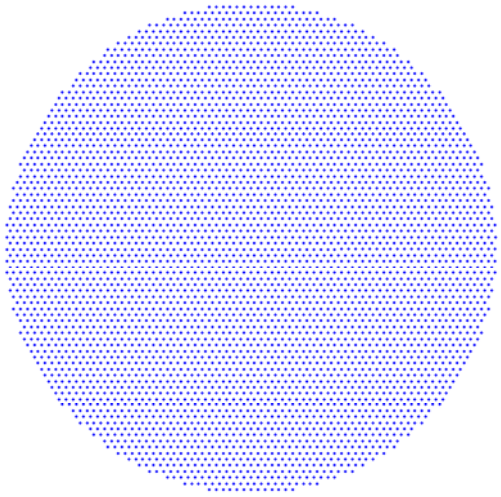

Figure 2: Element layout

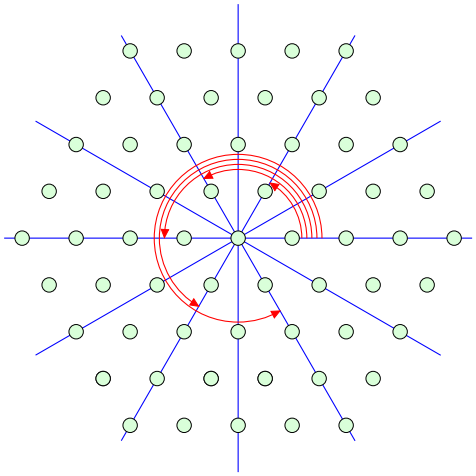

Figure 3: The optimized tapers (and array factors) are made invariant to various reflections and rotations simply to make optimizing a large array manageable.

2 Amplitude Tapers

In a well-matched transmit array the power into each element is proportional to the squared magnitude of the corresponding element weight, so the total power input to the array is proportional to the sum of the squared weight magnitudes, the energy in the weight function. In array optimization we are generally interested in maximizing the power density at some point in the far field, but should we do this assuming that the total power delivered to the elements is fixed or that there is some limit to the power that can be applied to any individual element? The answer depends on the hardware design, and so each design was optimized both ways. For reasons of convenience we actually fix the far-field power density at some point in space and minimize one of these two measures of element power. Fixing the far-field power density and minimizing total/peak-element power is equivalent, to within a common scale factor on the weights, to fixing the total/peak-element power and maximizing the far-field power density.

We use our MATLAB toolbox *Opt* [3] to design the amplitude tapers that follow. The *Opt* toolbox solves a particular class of convex-optimization problems in which a linear objective function is minimized subject to any number of constraints, each either a linear

constraint or a convex quadratic constraint.

The first two designs in this section are reference cases, the Uniform design (page 4) and the Mesa Reference design (page 8). Following these reference cases are two series of optimized designs: designs minimizing the energy in the element-weight function (Design 2.3 on page 13 through Design 2.9 on page 25) and designs minimizing the peak magnitude of the element-weight function (Design 2.10 on page 27 through Design 2.16 on page 39). For each series of amplitude taper optimizations, we include

- a simple, Taylor-like pencil beam design,
- a design with mesa constraints,
- a design combining the mesa constraints with a Taylor-like shelf constraint,
- a design combining the Taylor-like pencil beam and the brim constraints, and
- our final sombrero designs.

Design 2.1 A simple reference case: test the code

The reference design features uniform illumination. Each of the N weights is set to $1/N$ so that the array factor is unity, 0 dB, at boresight. No optimization is involved, but the code for computing and plotting the array factors and performance numbers is tested in a simple way here.

This reference design serves a second purpose as well, one based on it possessing a very special property. This reference design can be represented by 2D discrete-time Fourier pair $r_{\mathbf{n}} \leftrightarrow R(\mathbf{f})$, where taper $r_{\mathbf{n}}$ is a function of an integer two-vector element index $\mathbf{n}$. In particular, $r_{\mathbf{n}} = 1/N$ for $\mathbf{n}$ in the array and zero elsewhere. Using this reference design the signal power radiated in the boresight direction is proportional to $|R(0)|^2 = 1$, and the total power delivered to elements by the transmitter is proportional to $\|r\|^2 = \sum_{\mathbf{n}} |r_{\mathbf{n}}|^2 = 1/N$. Classically, boresight gain is taken as the ratio of these quantities $|R(0)|^2/\|r\|^2 = N$. Likewise, if taper $h_{\mathbf{n}} \leftrightarrow H(\mathbf{f})$ is used instead, its gain relative to that reference gain is

$$\frac{|H(0)|^2/\|h\|^2}{|R(0)|^2/\|r\|^2} = \frac{\left|\sum_{\mathbf{n}} h_{\mathbf{n}}\right|^2}{\|h\|^2\, N} = \frac{\left|\sum_{\mathbf{n}} h_{\mathbf{n}} \dfrac{1}{N}\right|^2}{\|h\|^2}\, \frac{N^2}{N} = \frac{|\langle h, r\rangle|^2}{\|h\|^2\|r\|^2} \tag{1}$$

using on the right inner product $\langle h, r\rangle = \sum_{\mathbf{n}} h_{\mathbf{n}} r_{\mathbf{n}}^*$. The point of this seemingly odd formulation of the gain improvement is that the ratio on the right cannot exceed unity, by the famous inequality of Cauchy, Schwarz, and Bunyakovsky. Therefore, no taper can improve on the boresight gain of this reference case, so for each design to follow we give the dB distance below this gain bound, classically referred to as taper loss, as

$$\langle \text{weight-energy taper loss} \rangle = -10 \log_{10} \frac{|\langle h, r\rangle|^2}{\|h\|^2\|r\|^2}. \tag{2}$$

This reference case also serves as the gain bound in the peak-element power sense. If we replace the element energy $\|h\|^2$ with the peak element magnitude $|h_{\text{max}}|^2$,

$$\frac{|H(0)|^2/|h_{\text{max}}|^2}{|R(0)|^2/|r_{\text{max}}|^2} = \frac{\left|\sum_{\mathbf{n}} h_{\mathbf{n}}\right|^2}{|h_{\text{max}}|^2\, N^2}. \tag{3}$$

But the numerator is equal to $\langle h, r\rangle^2/|r_{\text{max}}|^2$, so for each design we can report the dB distance below the gain bound as

$$\langle \text{max-weight taper loss}\rangle = -10\log_{10}\frac{|\langle h, r\rangle|^2}{|h_{\text{max}}|^2 N^2 |r_{\text{max}}|^2}. \tag{4}$$

Array factors are plotted in what is often and somewhat confusingly called either sine space or direction-cosine space. The far-field plane wave radiated with 3D radian vector wavenumber $2\pi\mathbf{k}$ has amplitude proportional to $\Phi(\mathbf{k})H\big((\mathbf{k}\lambda - \mathbf{s})^{\mathrm{T}}\mathbf{B}\big)$, where $\Phi(\mathbf{k})$ is the embedded element pattern and $H\big((\mathbf{k}\lambda - \mathbf{s})^{\mathrm{T}}\mathbf{B}\big)$ is the phase steered array factor of interest. Here $H(\mathbf{f})$ is the 2D discrete-time Fourier transform of the element weights $h_{\mathbf{n}}$, $\mathbf{s}$ is a unit vector in the steering direction, and $\mathbf{B}$ is a dimensionless 3×2 matrix characterizing the geometry of the element-layout grid. For a plane wave, normalized wavenumber $\mathbf{k}\lambda$ is a unit vector, but difference $\mathbf{k}\lambda - \mathbf{s}$ is not and can have a vector length approaching two. For this reason, we plot $H(\mathbf{k}^{\mathrm{T}}\lambda\mathbf{B})$ without restriction to the unit-vector case. Decomposition $\mathbf{k} = \underline{\mathbf{k}} + \mathbf{k}_{\perp}$ into array plane and perpendicular boresight components allows us to take advantage of the orthogonality of $\mathbf{k}_{\perp}$ to the columns of $\mathbf{B}$, both of which always lie in the array plane, through the resulting fact that $\mathbf{k}^{\mathrm{T}}\mathbf{B} = \underline{\mathbf{k}}^{\mathrm{T}}\mathbf{B}$. To plot $20\log_{10}|H(\mathbf{k}^{\mathrm{T}}\mathbf{B})|$ then, we will plot $20\log_{10}|H(\underline{\mathbf{k}}^{\mathrm{T}}\mathbf{B})|$ versus components of $\underline{\mathbf{k}}$ in the azimuth and elevation directions, and most often we will write the array factor as $|H(\underline{\mathbf{k}}^{\mathrm{T}}\mathbf{B})|$ as well.

The array factor is displayed at three different zoom levels in the first column of each figure.

galaxy zoom: A view of the array factor showing several periods.

world zoom: A big-picture view of the array factor. The latitude and longitude lines represent elevation and azimuth respectively, and the interior of the "world" is the visible region, the part of the array factor corresponding to physical directions. Elevation and azimuth lines are spaced at 15° intervals.

nation zoom 60 dB: A close-up view of the array factor showing details of the transition region. The plot spans -7.5° to 7.5° in elevation and azimuth, with a color scale of 60 dB. Elevation and azimuth lines are spaced at 1° intervals. The dB color scale uses contrasting colors for the -3 dB and -2 dB levels in order to make the associated beamwidths visible.

nation zoom 4 dB: A close-up view of the array factor showing details of the mesa, with a color scale of 5 dB. The dB color scale uses contrasting colors for the -3 dB and -2 dB levels in order to make the associated beamwidths visible.

slice plot: An array-factor slice plotted on both a linear and dB scale. The slice shown is from boresight to the edge of the visible region along elevation. This plot depicts qualitative behavior of the array factor and is particularly helpful when the optimization behavior is unexpected.

element weight vs. radius: The element weights are plotted versus the radius. Due to the symmetry of the problem specifications, none of the optimal amplitude weights have nonzero imaginary components, so all phases are 0° or 180°. Negative and nonnegative element weights are different colors (or will be for designs with weights of both polarities).

element weights: The element weights are plotted in 3D perspective. (This plot is not particularly revealing for this design, but will be for others to follow.)

The reported taper loss and taper efficiency numbers are two different ways of expressing the same measurement. They are not two different measurements.

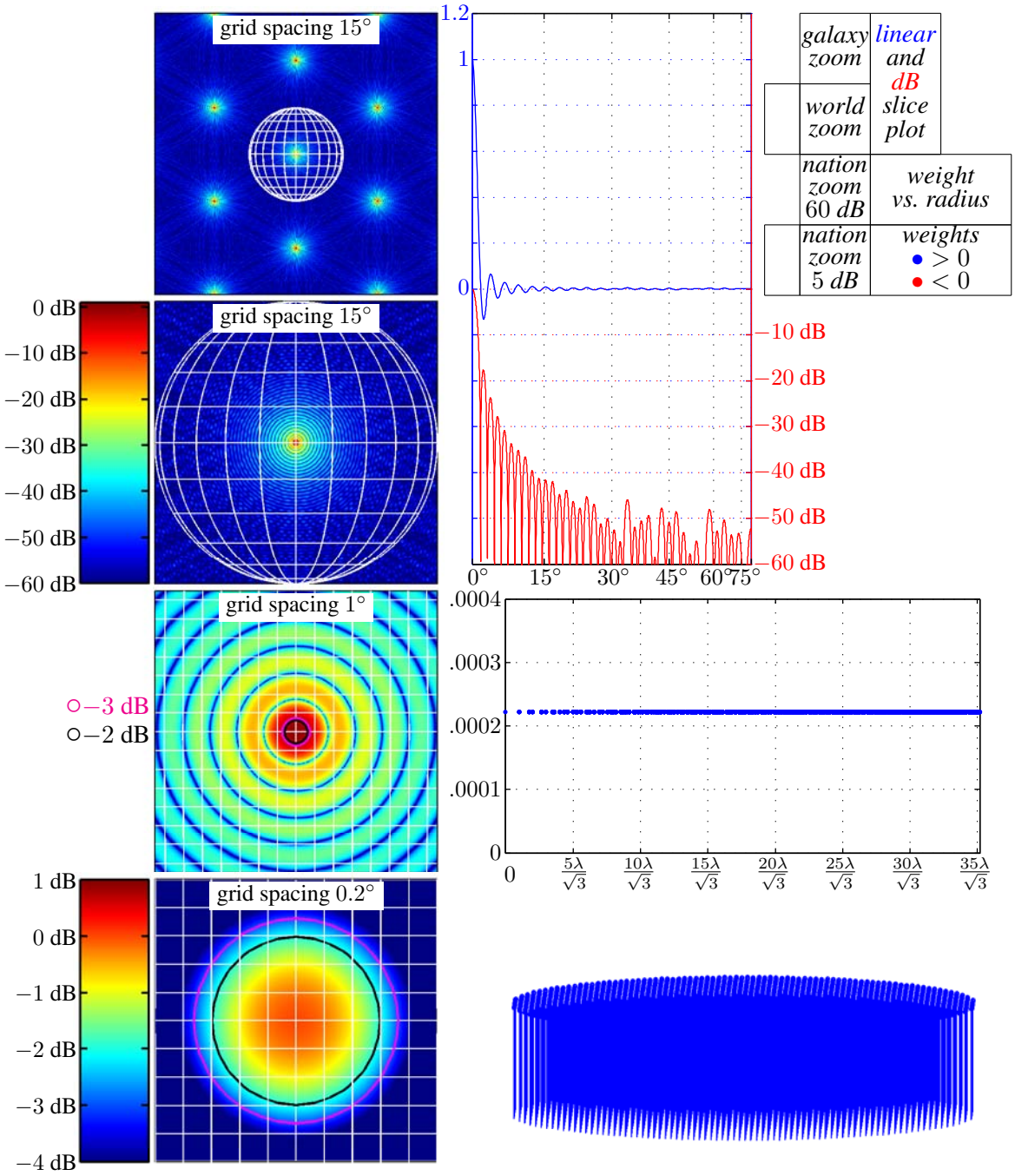

Results:

weight-energy taper loss (weight-energy taper efficiency)	0 dB	(100%)
max-weight taper loss (max-weight taper efficiency)	0 dB	(100%)

Figure 4: Uniform element weights

Design 2.2 A mesa reference case

The taper losses of (2) and (4) jump upward when we add a mesa to the designs because of the large increase in noise-gain factor

$$\|h\|^2 = \sum_{\mathbf{n}} |h_{\mathbf{n}}|^2 = \int_{\substack{\text{unit}\\ \text{square}}} |H(\mathbf{f})|^2 \, d\mathbf{f} = \lambda^2 |\mathbf{B}^{\mathrm{T}}\mathbf{B}|^{1/2} \int_{\substack{\text{one}\\ \text{period}}} |H(\underline{\mathbf{k}}^{\mathrm{T}}\lambda\mathbf{B})|^2 \, d\underline{\mathbf{k}},$$

where $d\mathbf{f}$ is differential area in two-vector $\mathbf{f}$ and $d\underline{\mathbf{k}}$ is differential area in the array-plane component $\underline{\mathbf{k}}$ of three-vector $\mathbf{k}$. The integral on the right becomes much larger when $H(\underline{\mathbf{k}}^{\mathrm{T}}\lambda\mathbf{B})$ is given a near-unity value over the entire mesa rather than over a pencil beam as before. What this means is that the Design 2.1 reference is a poor choice for tapers with mesas: How do you know if a taper loss of 12 dB is good or not? It turns out that we can extend the notion of taper loss to explicitly account for a mesa in a way that is particularly clean for amplitude tapers.

How do we characterize the mesa mathematically? Array factors are plotted as functions of the array-plane component $\underline{\mathbf{k}}$ of three-vector $\mathbf{k}$, so the mesa is actually a set of array-plane values. Each such value can be written as a weighted combination of a pair of linearly independent array-plane basis vectors. The columns of basis matrix $\mathbf{B}$ are such a pair, but it is convenient here to instead use the rows of $\mathbf{B}^+$, the Moore-Penrose pseudoinverse of $\mathbf{B}$ that is formally given as $\mathbf{B}^+ = (\mathbf{B}^{\mathrm{T}}\mathbf{B})^{-1}\mathbf{B}^{\mathrm{T}}$ and that is realized in matlab with the `pinv()` function. Its rows are in the array plane because each is just a linear combination of the basis-vector columns of $\mathbf{B}$, and this new basis is appealing because if we represent an array-plane value $\underline{\mathbf{k}}$ using a row two-vector $\mathbf{f}$ of coordinates so that $\underline{\mathbf{k}}^{\mathrm{T}} = \frac{1}{\lambda}\mathbf{f}\mathbf{B}^+$, the simplifying relationship $\underline{\mathbf{k}}^{\mathrm{T}}\lambda\mathbf{B} = \mathbf{f}\mathbf{B}^+\mathbf{B} = \mathbf{f}$ results.

Choosing the mesa now amounts to choosing a set of $\mathbf{f}$ vectors. We will soon be taking averages across the mesa, and averages are nicely handled by the expected values of probability theory, so let us suppose that $\mathbf{f}$, and implicitly $\underline{\mathbf{k}}$ as well, is a random vector distributed probabilistically across one array-factor period and, in particular, with probability concentrated in the mesa. Then

$$\begin{matrix}\text{average}\\ \text{amplitude gain}\end{matrix} = \frac{E|H(\underline{\mathbf{k}}^{\mathrm{T}}\lambda\mathbf{B})|}{\|h\|} = \frac{E|H(\mathbf{f})|}{\|h\|}.$$

By distributing probability in the mesa according to the weighting desired in the average, we could in principle obtain a weighted average. We do not do so, however.

Consider some specific cases.

Case: single-point mesa. If $\mathbf{f} = 0$ with probability one,

$$\begin{matrix}\text{average}\\ \text{amplitude gain}\end{matrix} = \frac{|H(0)|}{\|h\|}$$

For this degenerate mesa the average amplitude gain is just the boresight gain used to derive weight-energy taper loss in Design 2.1 (which begins on page 4). There is no reason to compute average amplitude gain separately with the single point considered as a mesa.

Case: mesa defined by a pdf. This is the main case of interest. Suppose the probability of $\mathbf{f}$ falling into a subset $\mathcal{F}$ of the unit square is

$$P\big[\mathbf{f}\in\mathcal{F}\big] = \int_{\mathcal{F}} p(\mathbf{f})\, d\mathbf{f},$$

where $d\mathbf{f}$ is differential area in the $\mathbf{f}$ plane so that $p(\mathbf{f})$ on the unit square is a probability density function (pdf) for $\mathbf{f}$. Then let $p(\mathbf{f})$ be periodic with the unit square as its period, so that it can be inverse Fourier transformed. After inverse transforming $|H(\mathbf{f})|$ as well, we can use 2D Fourier pairs $\bar{h}_{\mathbf{n}} \leftrightarrow |H(\mathbf{f})|$ and $\phi_{\mathbf{n}} \leftrightarrow p(\mathbf{f})$ along with Parseval's relation and $\|\bar{h}\|^2 = \|h\|^2$, which is obvious in the frequency domain, to write

$$\begin{aligned}\underset{\text{amplitude gain}}{\text{average}} &= \frac{1}{\|h\|}\int_{\substack{\text{unit}\\ \text{square}}} |H(\mathbf{f})|\, p(\mathbf{f})\, d\mathbf{f} \qquad (5)\\ &= \frac{\langle \bar{h}, \phi\rangle}{\|\bar{h}\|}.\end{aligned}$$

There are two subcases.

Subcase: zero-phase taper. The amplitude tapers of this report not only give each weight in the taper a zero phase, the design symmetries imposed also give each point of the associated array factor a zero phase. Though somewhat confusing, the custom in signal processing is to refer to tapers with the latter property as zero-phase tapers (or filters) or, less precisely, as linear-phase tapers (or filters). Typically a zero-phase taper not only has $H(\mathbf{f})$ real everywhere in the mesa, generally in the mesa it also has $H(\mathbf{f}) > 0$ so that $|H(\mathbf{f})| = H(\mathbf{f})$ and

$$\underset{\text{amplitude gain}}{\text{average}} = \frac{1}{\|h\|}\int_{\substack{\text{unit}\\ \text{square}}} H(\mathbf{f})\, p(\mathbf{f})\, d\mathbf{f} = \frac{\langle h, \phi\rangle}{\|h\|}.$$

Since $h_{\mathbf{n}} = 0$ for $\mathbf{n}$ not corresponding to actual array elements, inner product $\langle h, \phi\rangle = \sum_{\mathbf{n}} h_{\mathbf{n}}\phi^*_{\mathbf{n}}$ has many zero terms. We can just as well decompose ϕ as $\phi_{\mathbf{n}} = \underline{\phi}_{\mathbf{n}} + \phi_{\perp\mathbf{n}}$, where $\underline{\phi}_{\mathbf{n}}$ and $\phi_{\perp\mathbf{n}}$ can be nonzero only for $\mathbf{n}$ corresponding to elements actually inside and outside the array respectively, and write $\langle h, \phi\rangle = \langle h, \underline{\phi}\rangle$. It is then useful to consider the ratio

$$\frac{\underset{\text{amplitude gain}}{\text{average}}}{\|\underline{\phi}\|} = \frac{\langle h, \underline{\phi}\rangle}{\|h\|\|\underline{\phi}\|},$$

because by the Cauchy-Schwarz-Bunyakovsky inequality the quantity on the right will never exceed one, but we can make it equal to one by setting $h = \underline{\phi}$. We characterize the closeness of a mesa design to this optimum, using terminology loosely (because technically we are averaging the gain and not the loss),

by reporting

$$\langle \text{average mesa taper loss} \rangle = -20 \log_{10} \frac{\text{average amplitude gain}}{\|\underline{\phi}\|} = -20 \log_{10} \frac{|\langle h, \underline{\phi} \rangle|}{\|h\| \|\underline{\phi}\|} \tag{6}$$

with confidence that in this zero-phase subcase it must be nonnegative.

Subcase: a taper with phase variation. Later, in Section 3 (beginning on page 41) on phase-only tapers, we will continue to report (6) but with the average amplitude gain calculated by numerically evaluating the integral in (5). In this subcase we have no Cauchy-Schwarz-Bunyakovsky bound on the values this average mesa taper loss might take.

The Airy taper. We give our zero-phase tapers mesas by defining pdf $p(\mathbf{f}) = p(\underline{\mathbf{k}}^{\mathrm{T}} \lambda \mathbf{B})$ to be constant inside a circle in $\underline{\mathbf{k}}$ of mesa radius k_r and to be zero outside that circle. An inverse 2D discrete-time Fourier transform of $p(\mathbf{f})$ and subsequent restriction of $\phi_{\mathbf{n}}$ to the array aperture then gives $\underline{\phi}_{\mathbf{n}}$ as a sampled version

$$\underline{\phi}_{\mathbf{n}} = 2 \, \mathrm{jinc}(2\pi k_r \|\mathbf{B} \lambda \mathbf{n}\|) \tag{7}$$

of the Airy pattern from optics, using a jinc function defined using a Bessel function:

$$\mathrm{jinc}(x) = \begin{cases} J_1(x)/x & \text{for } x \neq 0, \\ \lim\limits_{x \downarrow 0} J_1(x)/x = \frac{1}{2} & \text{for } x = 0. \end{cases}$$

The scaling has been chosen so that $\underline{\phi}_0 = \int_{\text{square}} p(\mathbf{f}) \, d\mathbf{f} = 1$ as required.

Given that our array size is fixed, k_r is the one free parameter in the definition of $\underline{\phi}_{\mathbf{n}}$. Average mesa taper loss is presented for every taper in this report for which a mesa is an intended design feature, and for all amplitude tapers a common mesa radius parameter k_r is used in calculating $\underline{\phi}_{\mathbf{n}}$. Just as we do not expect a filter's ripple bandwidth, 3 dB bandwidth, and noise bandwidth to be the same, here we do not assume that k_r should exactly match the design radius used to specify the mesa size in the optimization constraints. Instead we determine this common value of k_r by computing the average mesa taper loss of Design 2.4 for a range of k_r values. The result is shown in Figure 5. The lowest average mesa taper loss is obtained with $k_r = 0.0882/\lambda$, so that value is used for calculating average mesa taper loss for each amplitude-taper design that has a mesa.

Of course taper loss is indifferent to scaling, so rather than take the scaling implied by $h = \underline{\phi}$, we can if we wish set the boresight gain to approximately unity. The scaling of Fourier pair $\phi_{\mathbf{n}} \leftrightarrow p(\mathbf{f})$ yields $\int_{\text{square}} p(\mathbf{f}) \, d\mathbf{f} = 1$, so if we scale $\underline{\phi}_{\mathbf{n}}$, $\phi_{\mathbf{n}}$, and $p(\underline{\mathbf{k}}^{\mathrm{T}} \lambda \mathbf{B})$ by $|\mathbf{B}^{\mathrm{T}} \mathbf{B}|^{1/2} \pi (k_r \lambda)^2$, after scaling the last of the three will have unit height in the mesa. After scaling, the first of the three becomes our reference taper and will transform to an array factor of approximately unit mesa height but featuring truncation-related ripples and sidelobes.

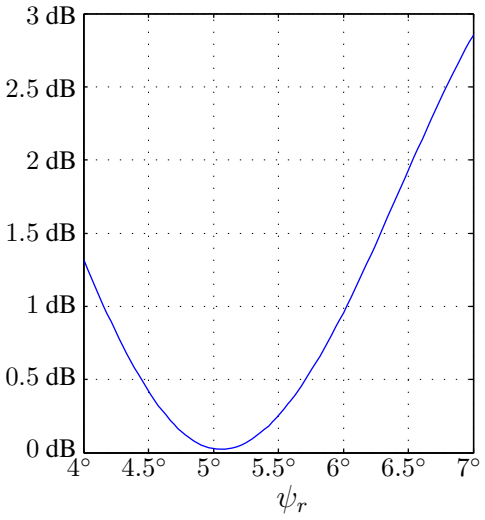

Figure 5: Average mesa taper loss of Design 2.4 versus ψ_r, the angular radius of the mesa. We choose the direction-cosine-space mesa radius $k_r = \sin(\psi_r)/\lambda$ in (7) to minimize this Design 2.4 average mesa taper loss.

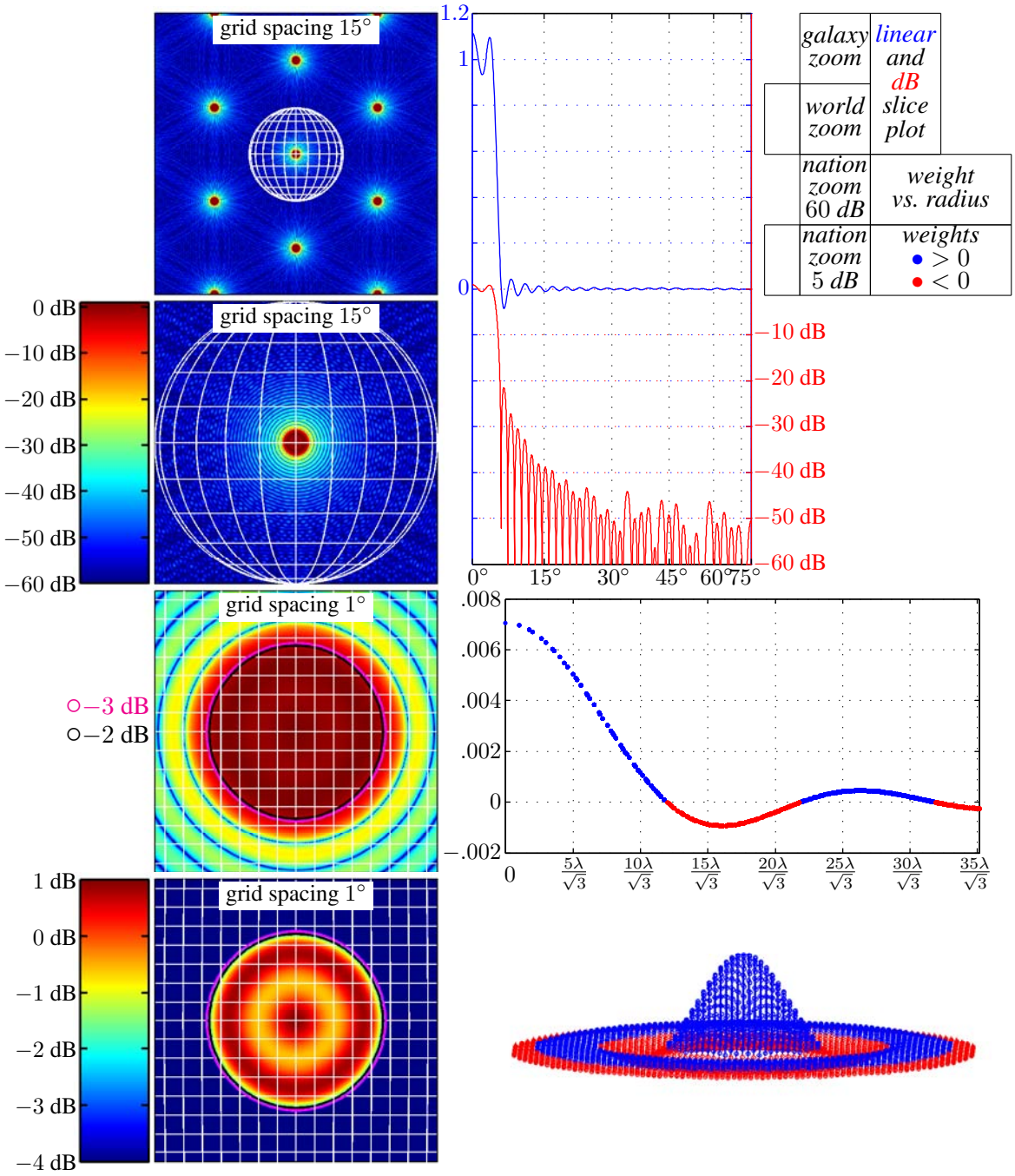

Results:

weight-energy taper loss (weight-energy taper efficiency)	13.80 dB	(4.17%)
max-weight taper loss (max-weight taper efficiency)	29.09 dB	(0.12%)
average mesa taper loss (average mesa taper efficiency)	0 dB	(100%)

Figure 6: Reference design for all amplitude tapers with mesas

Design 2.3 Weight-energy minimization, Taylor-like pencil beam

The first set of optimizations minimize the array-factor energy (or weight energy, thanks to Parseval). Note that for the examples with mesas this is not exactly the same as minimizing the weight-energy taper loss since the boresight gain is not explicitly fixed. Nor is it equivalent to minimizing average mesa taper loss, because the average mesa gain is not explicitly fixed. This can lead to some slightly unexpected results when comparing designs, as shown later in the discussions for Design 2.8 and Design 2.12. However, the peak constraints on the mesa do approximately fix both the boresight and average mesa gains, and thus the net result is to approximately minimize the two taper losses that depend on total weight energy.

This design is a pencil beam with a Taylor-like response. The following constraints are applied to the filter (• on the array-factor plots):

- upperbound the array-factor sidelobes by -35 dB over the shelf region, from 2.5° outward.
- constrain the array factor at boresight to 0 dB.

The element weights are nonnegative.

The points where constraints are applied are visible on each of the array-factor plots (•). Due to the symmetries in the problem formulation (Figure 3), these points, which are spread across roughly $1/12$ of the array-factor period, constrain nearly the entire universe. Of course if we were to remove those required array-factor symmetries from the formulation, for example to enable the inclusion of some asymmetric sidelobe limits, the number of variables optimized would be much larger.

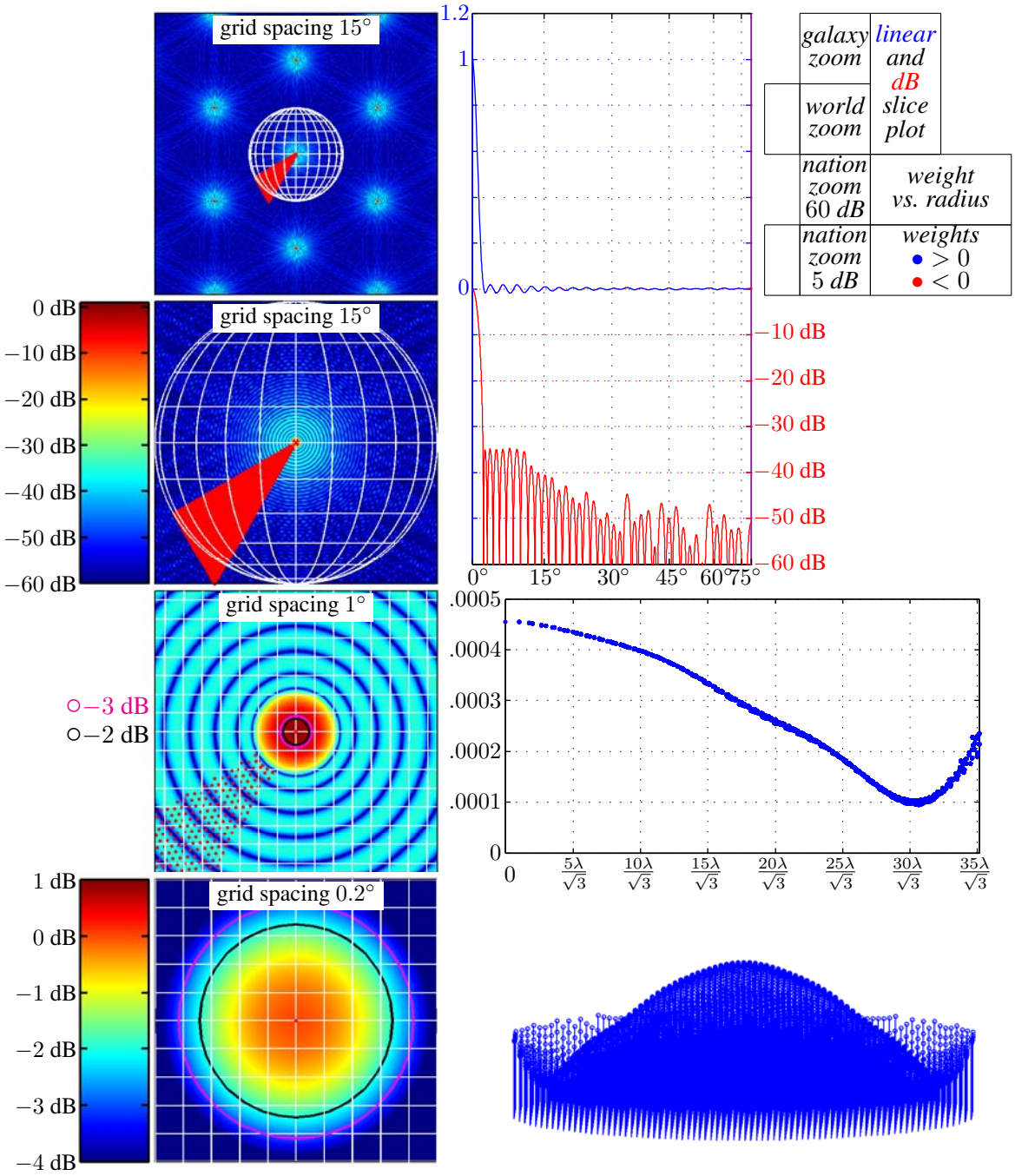

Results:

weight-energy taper loss (weight-energy taper efficiency)	0.83 dB	(82.62%)
max-weight taper loss (max-weight taper efficiency)	6.25 dB	(23.72%)
weight-energy level	−35.71 dB	

Figure 7: Weight-energy minimization of Taylor-like pencil beam

Design 2.4 Weight-energy minimization, mesa constraint

Next, we test the mesa constraint on our design. The mainbeam is broadened to 4.25° so that a cluster of approximately 19 pencil beams will fit inside the mesa (Figure 8). The following constraint is applied to the filter (•) on the array-factor plots):

- bound the array factor between -1 dB and 0 dB in the mesa region, from boresight to 4.25°.

The weight-energy taper loss is 14.99 dB. This large number results from the dissimilarity between the present wide beam and the reference pencil beam of Design 2.1. The average mesa taper loss is a more appropriate measure because it compares to the mesa-reference wide beam of Design 2.2. The average mesa taper loss is 0.02 dB. That it is very small is no surprise, because in Figure 5 we fixed the mesa radius of Design 2.2 to minimize the weight-energy taper loss of this very design. The element weights are both negative and nonnegative.

If desired, one could eliminate the hexagonal rays that extend from the mainbeam by modifying the shape of the circular array.

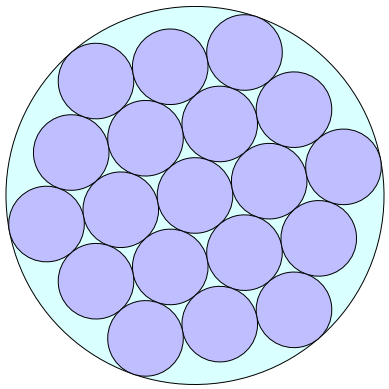

Figure 8: 19 beams packed into a hexagonal cluster.

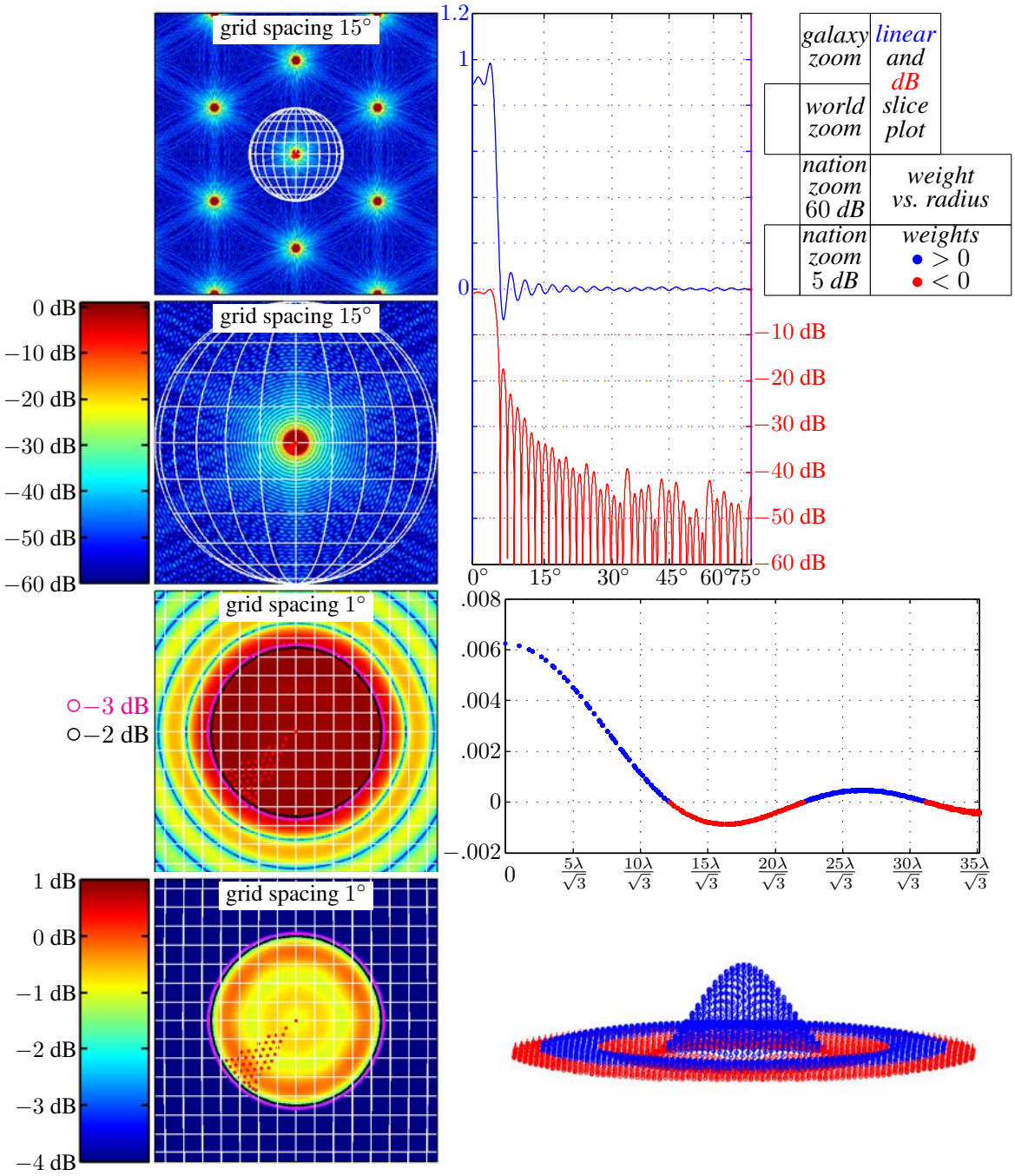

Results:

weight-energy taper loss (weight-energy taper efficiency)	14.99 dB	(3.17%)
max-weight taper loss (max-weight taper efficiency)	29.97 dB	(0.10%)
average mesa taper loss (average mesa taper efficiency)	0.02 dB	(99.47%)
weight-energy level	−22.55 dB	

Figure 9: Weight-energy minimization with a mesa constraint

Design 2.5 Weight-energy minimization, mesa constraint, -35 dB shelf constraint

Here we combine the mesa constraint with the Taylor-like shelf constraint to get a broader beam with a Taylor-like response. The following constraints are applied to the filter (•) on the array-factor plots):

- bound the array factor between -1 dB and 0 dB in the mesa region, from boresight to $4.25°$.
- upperbound the array-factor sidelobes by -35 dB over the shelf region, from $6.8°$ outward.

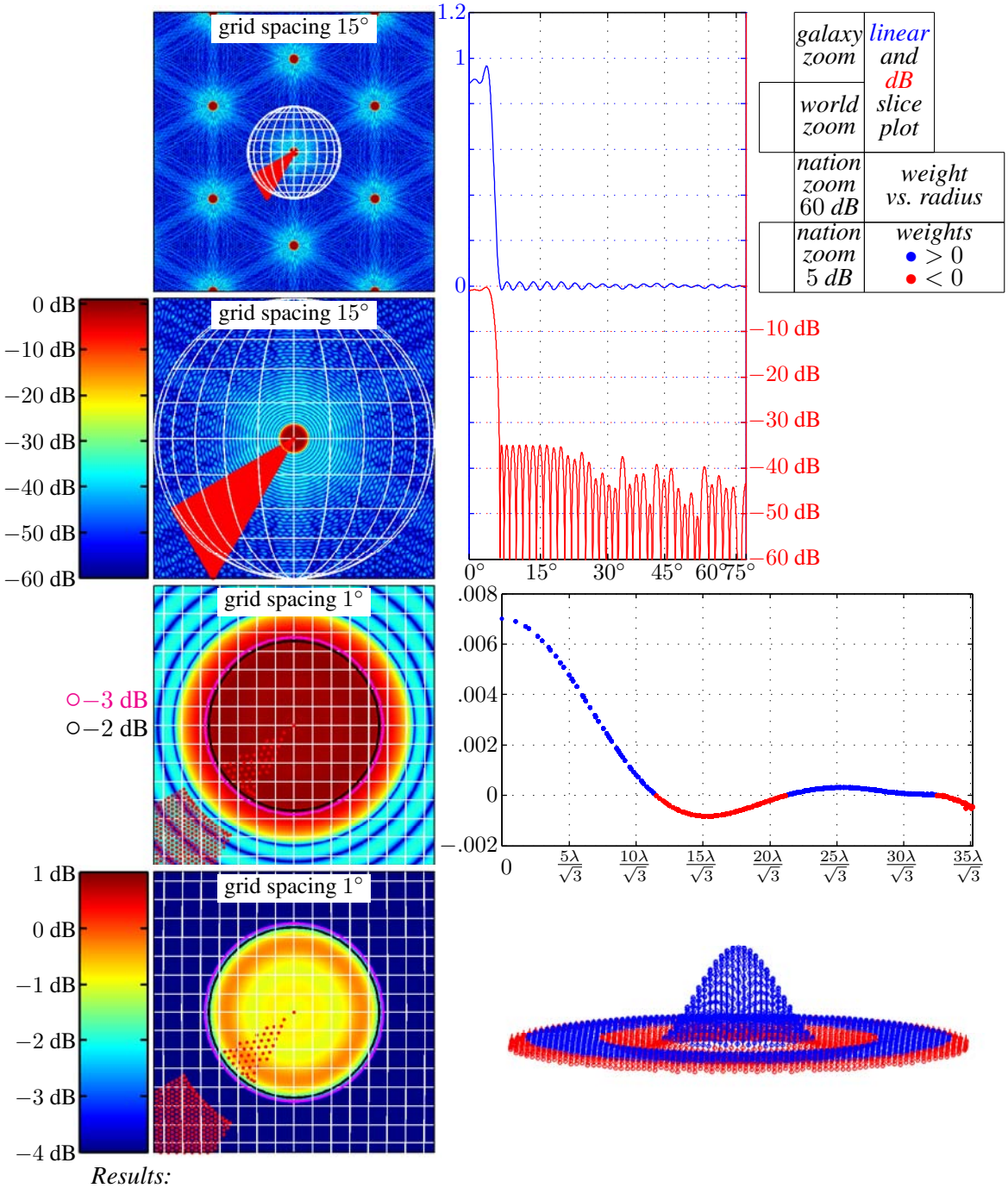

Results:

weight-energy taper loss (weight-energy taper efficiency)	15.11 dB	(3.08%)
max-weight taper loss (max-weight taper efficiency)	30.98 dB	(0.08%)
average mesa taper loss (average mesa taper efficiency)	0.06 dB	(98.60%)
weight-energy level	−22.43 dB	

Figure 10: Weight-energy minimization with a mesa constraint and a −35 dB Taylor-like shelf constraint

Design 2.6 Weight-energy minimization, mesa constraint, -23 dB shelf constraint

Here, we change the shelf height from -35 dB, a reasonable shelf height for a Taylor-like array, to -23 dB, the target height of the brim for our sombrero designs. The following constraints are applied to the filter (•) on the array-factor plots):

- bound the array factor between -1 dB and 0 dB in the mesa region, from boresight to $4.25°$.
- upperbound the array-factor sidelobes by -23 dB over the shelf region, from $6.8°$ outward.

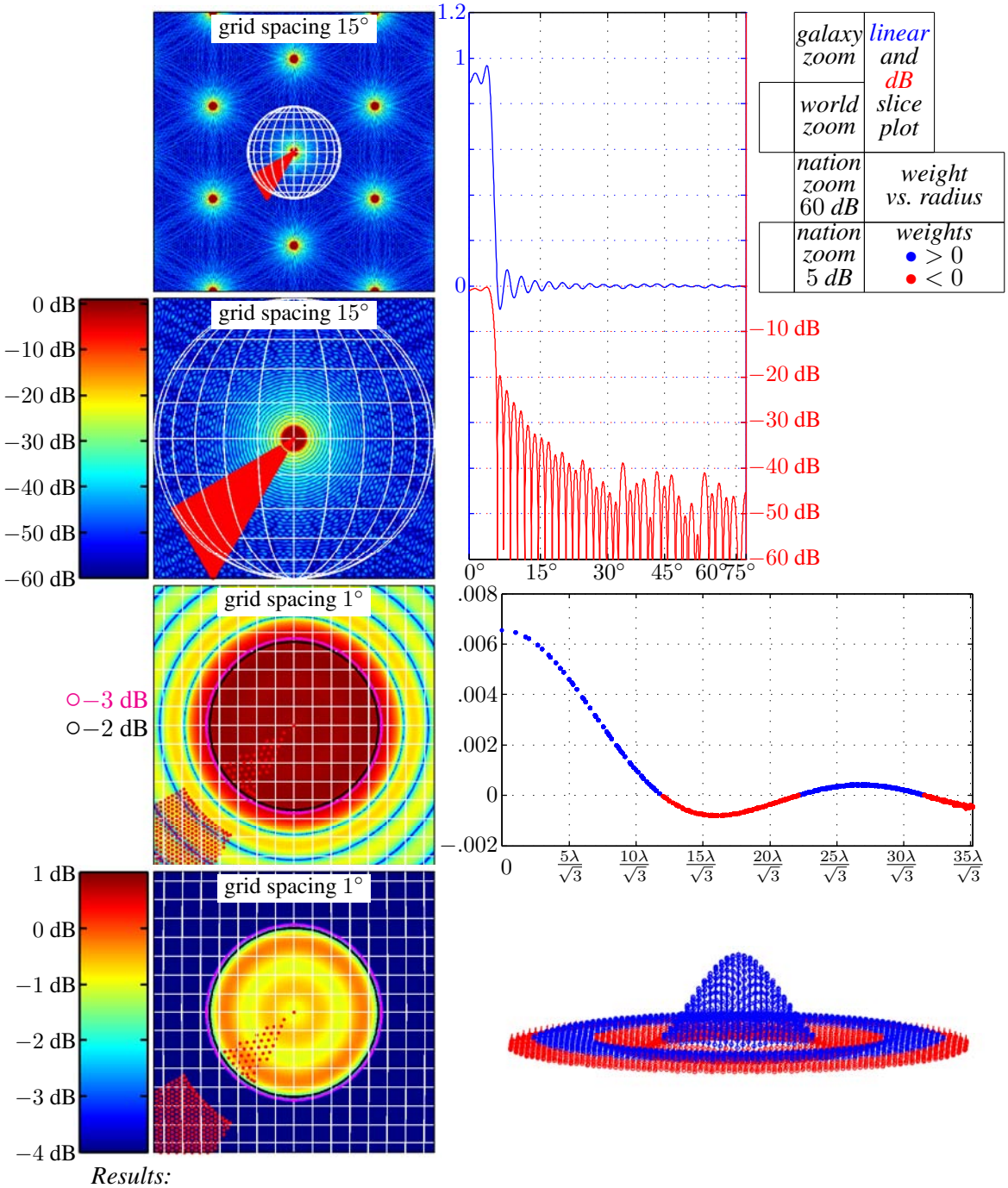

Results:

weight-energy taper loss (weight-energy taper efficiency)	15.00 dB	(3.16%)
max-weight taper loss (max-weight taper efficiency)	30.20 dB	(0.10%)
average mesa taper loss (average mesa taper efficiency)	0.02 dB	(99.52%)
weight-energy level	−22.54 dB	

Figure 11: Weight-energy minimization with a mesa constraint and a −23 dB Taylor-like shelf constraint

Design 2.7 Weight-energy minimization, Taylor-like pencil beam, 30° brim constraints

Here we go back to a pencil beam design (we remove the mesa constraints) and add the brim constraints (the pedestal and shelf constraints in Figure 1) to produce a sombrero-shaped array factor with a pencil-beam mesa. The following constraints are applied to the filter (•) on the array-factor plots):

- constrain the array factor at boresight to 0 dB.
- upperbound the array-factor sidelobes by -23 dB over the shelf region, from 2.5° outward (•) on the array-factor plots).
- lowerbound the array factor by -25 dB in the pedestal region, from 6.8° to 30° (○ on the array-factor plots).

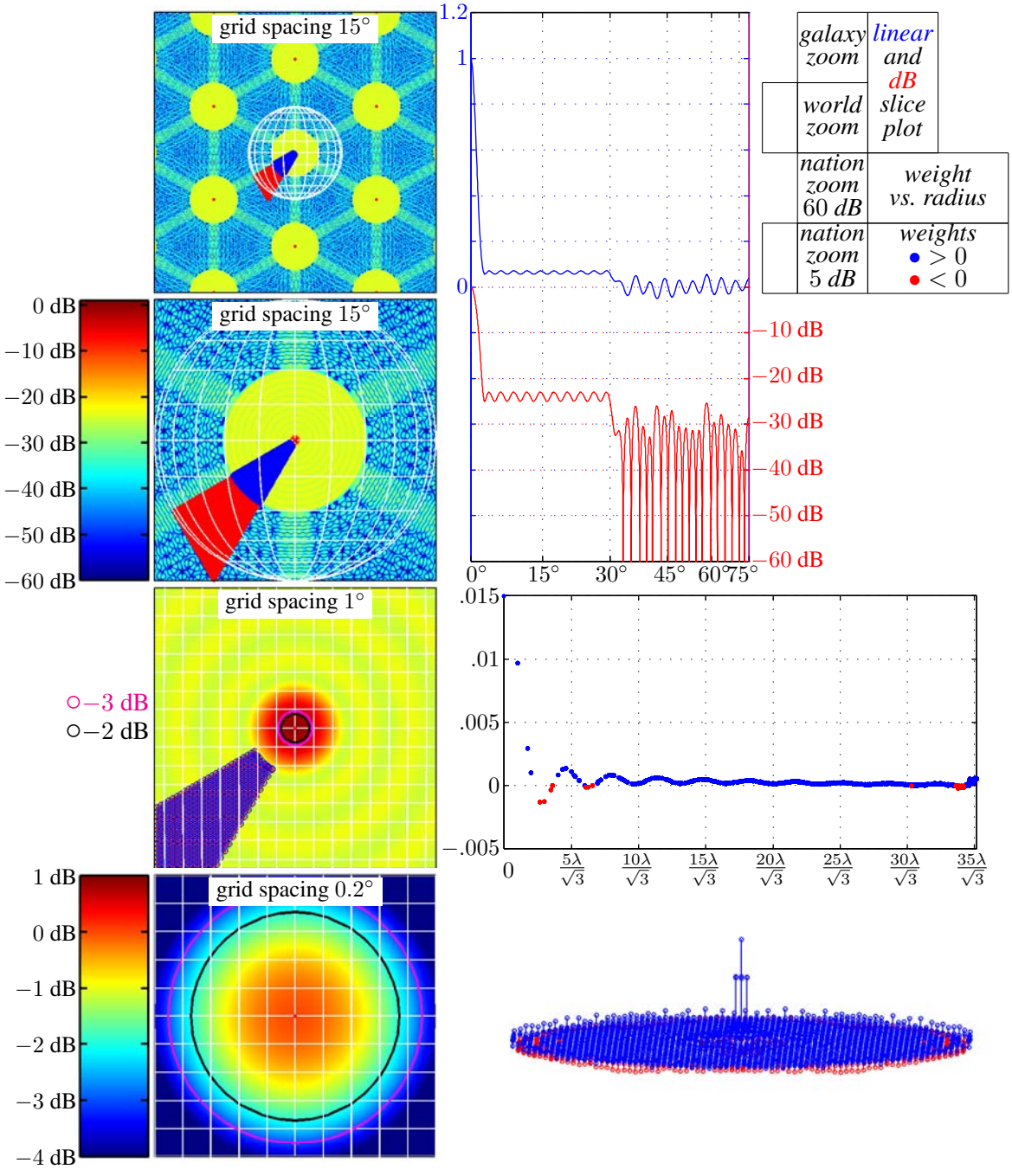

Results:

weight-energy taper loss (weight-energy taper efficiency)	8.13 dB	(15.37%)
max-weight taper loss (max-weight taper efficiency)	37.01 dB	(0.02%)
weight-energy level	−28.41 dB	

Figure 12: Weight-energy minimization of a Taylor-like pencil beam with 30° brim constraints.

Design 2.8 Weight-energy minimization, sombrero constraints, 30° brim

Next, mesa constraints are reintroduced to generate our desired sombrero pattern. The constraints for the sombrero pattern are:

- bound the array factor between -1 dB and 0 dB in the mesa region, from boresight to 4.25° (•) on the array-factor plots).
- upperbound the array-factor sidelobes by -23 dB over the shelf region, from 6.8° outward (•) on the array-factor plots).
- lowerbound the array factor by -25 dB in the pedestal region, from 6.8° to 30° (○ on the array-factor plots).

The constraints of this sombrero design include all of the constraints from the Taylor-like Mesa design (Design 2.6) plus one additional (pedestal) constraint. Therefore the set of possible (feasible) optimization outcomes of this sombrero design is a subset of the set of possible optimization outcomes of the Taylor-like mesa design. One would expect

$$\text{quality}\big(\text{best}(\langle\text{small set}\rangle)\big) \le \text{quality}\big(\text{best}(\langle\text{large set}\rangle)\big)$$

if $\langle\text{small set}\rangle \subset \langle\text{large set}\rangle$. It appears superficially that whether this expectation is met depends on the quality measure chosen. The

$$\langle\text{weight-energy taper loss}\rangle_{\text{dB}} = \begin{cases} 15.11 \text{ dB} & \text{Taylor-like Mesa design,} \\ 14.93 \text{ dB} & \text{Sombrero design,} \end{cases}$$

and

$$\langle\text{energy}\rangle_{\text{dB}} = \begin{cases} -22.43 \text{ dB} & \text{Taylor-like Mesa design,} \\ -21.66 \text{ dB} & \text{Sombrero design.} \end{cases}$$

The weight-energy taper loss results do not match our expectations, while the weight-energy levels do meet our expectations. The energy is actually minimized by the optimization, so the results there are not surprising. Relationship (1) can be written in decibel form as weight-energy taper loss to energy is

$$\langle\text{weight-energy taper loss}\rangle_{\text{dB}} = \langle\text{ideal gain}\rangle_{\text{dB}} + \langle\text{energy}\rangle_{\text{dB}} - 20\log_{10}\big|\langle\text{boresight array factor}\rangle\big|. \quad (8)$$

Ideal gain is not affected by the optimization, but the boresight-array-factor term can be. Here

$$-20\log_{10}|\langle\text{boresight array factor}\rangle| = \begin{cases} 1.00 \text{ dB} & \text{Taylor-like Mesa design,} \\ 0.05 \text{ dB} & \text{Sombrero design.} \end{cases}$$

If we use this to adjust the taper loss,

$$\langle\text{weight-energy taper loss}\rangle_{\text{dB}} - 20\log_{10}\big|\langle\text{boresight array factor}\rangle\big| = \begin{cases} 14.00 \text{ dB} & \text{Taylor-like Mesa design,} \\ 14.88 \text{ dB} & \text{Sombrero design,} \end{cases}$$

which behaves as expected.

We conclude from this array-factor design that it is possible to optimize a sombrero pattern for an array.

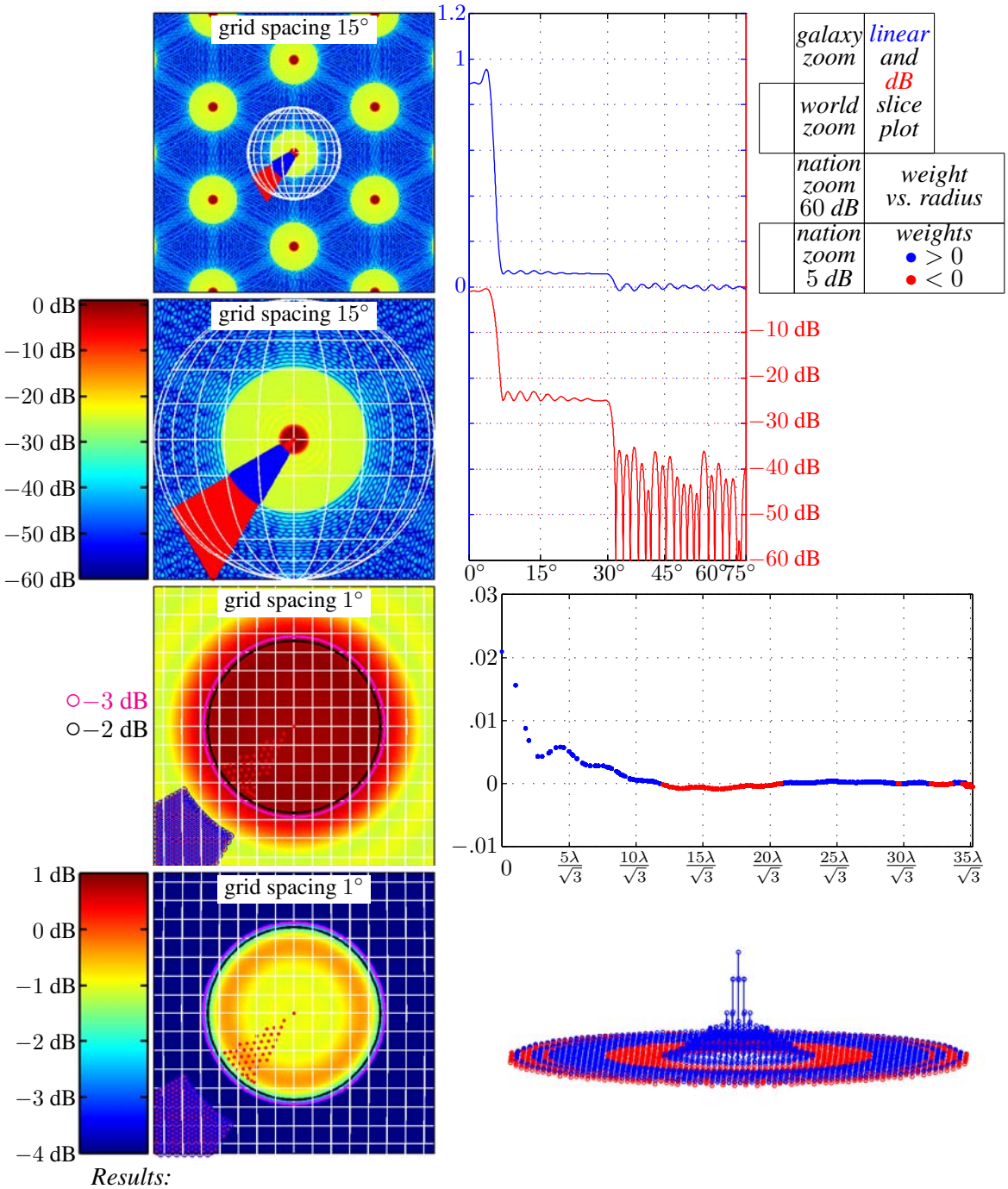

Results:

weight-energy taper loss (weight-energy taper efficiency)	15.86 dB	(2.60%)
max-weight taper loss (max-weight taper efficiency)	40.55 dB	(0.01%)
average mesa taper loss (average mesa taper efficiency)	0.75 dB	(84.23%)
weight-energy level	−21.68 dB	

Figure 13: Weight-energy minimization with sombrero constraints (30° brim)

Design 2.9 Weight-energy minimization, sombrero constraints, 45° brim

Here is another example of the sombrero pattern, with the brim extending out to 45°. The constraints for the sombrero pattern are:

- bound the array factor between -1 dB and 0 dB in the mesa region, from boresight to 4.25° (•) on the array-factor plots).
- upperbound the array-factor sidelobes by -23 dB over the shelf region, from 6.8° outward (•) on the array-factor plots).
- lowerbound the array factor by -25 dB in the pedestal region, from 6.8° to 45° (○ on the array-factor plots).

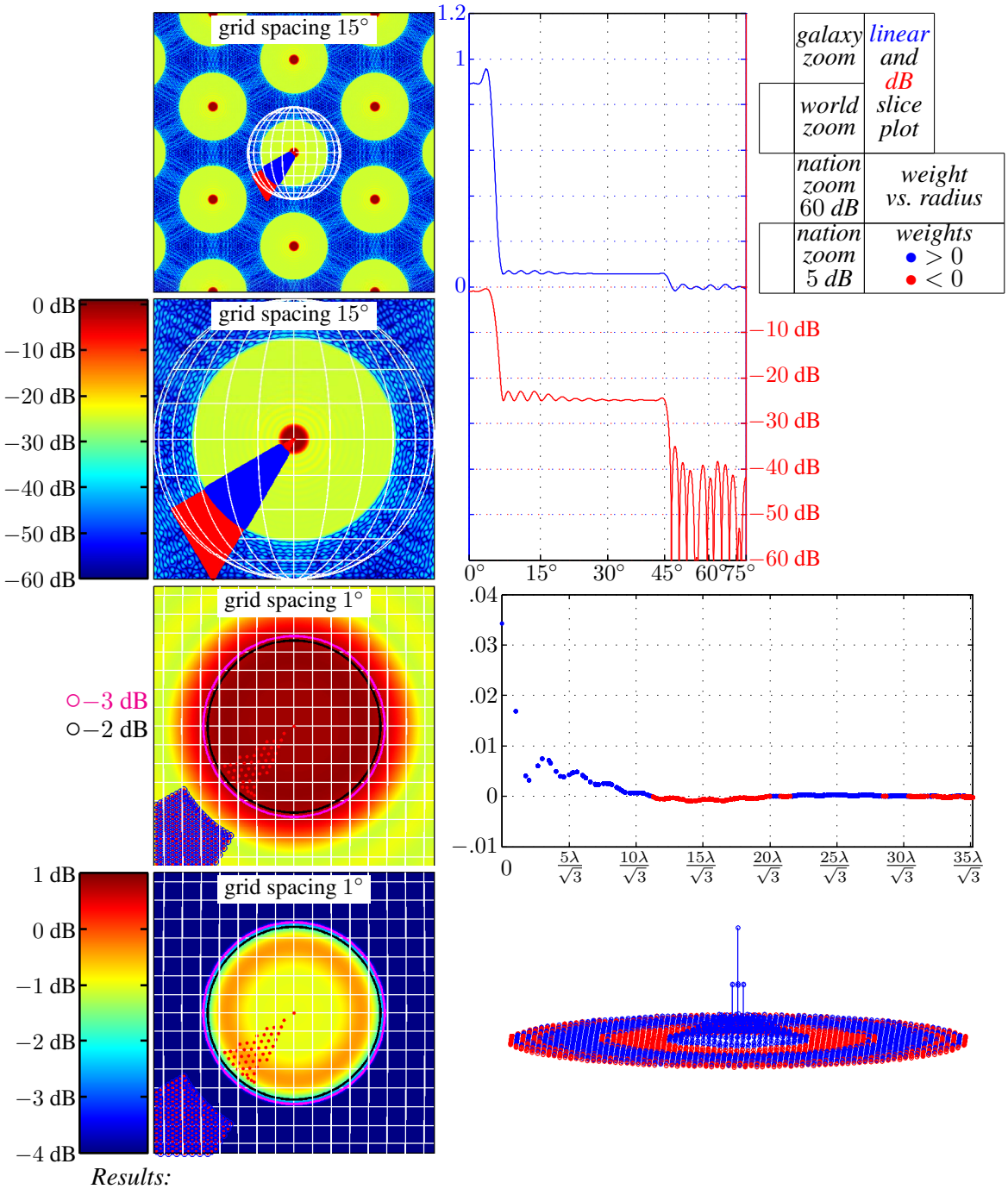

Results:

weight-energy taper loss (weight-energy taper efficiency)	16.32 dB	(2.33%)
max-weight taper loss (max-weight taper efficiency)	44.77 dB	(0.003%)
average mesa taper loss (average mesa taper efficiency)	1.20 dB	(75.86%)
weight-energy level	−21.22 dB	

Figure 14: Weight-energy minimization with sombrero constraints (45° brim)

Design 2.10 Max-weight optimization, Taylor-like pencil beam

The second set of optimizations minimize the peak magnitude of the element weights. From (3) we can obtain a relationship analogous to (8) but for the max-weight taper loss:

$$\langle \text{max-weight taper loss} \rangle_{\text{dB}} = \langle \text{ideal gain} \rangle_{\text{dB}} + 10 \log_{10}\big(N|h_{\text{max}}|^2\big) - 20 \log_{10}\big|\langle \text{boresight array factor} \rangle\big|. \quad (9)$$

This design is a pencil beam with a Taylor-like response. The following constraints are applied to the filter (•) on the array-factor plots):

- upperbound the array-factor sidelobes by -35 dB over the shelf region, from 2.5° outward.
- constrain the array factor at boresight to 0 dB.

Comparing to the weight-energy optimization with identical constraints (Design 2.3), note that the peak optimization buys us nothing (there is no visible change in the peak coefficient) and costs us weight energy.

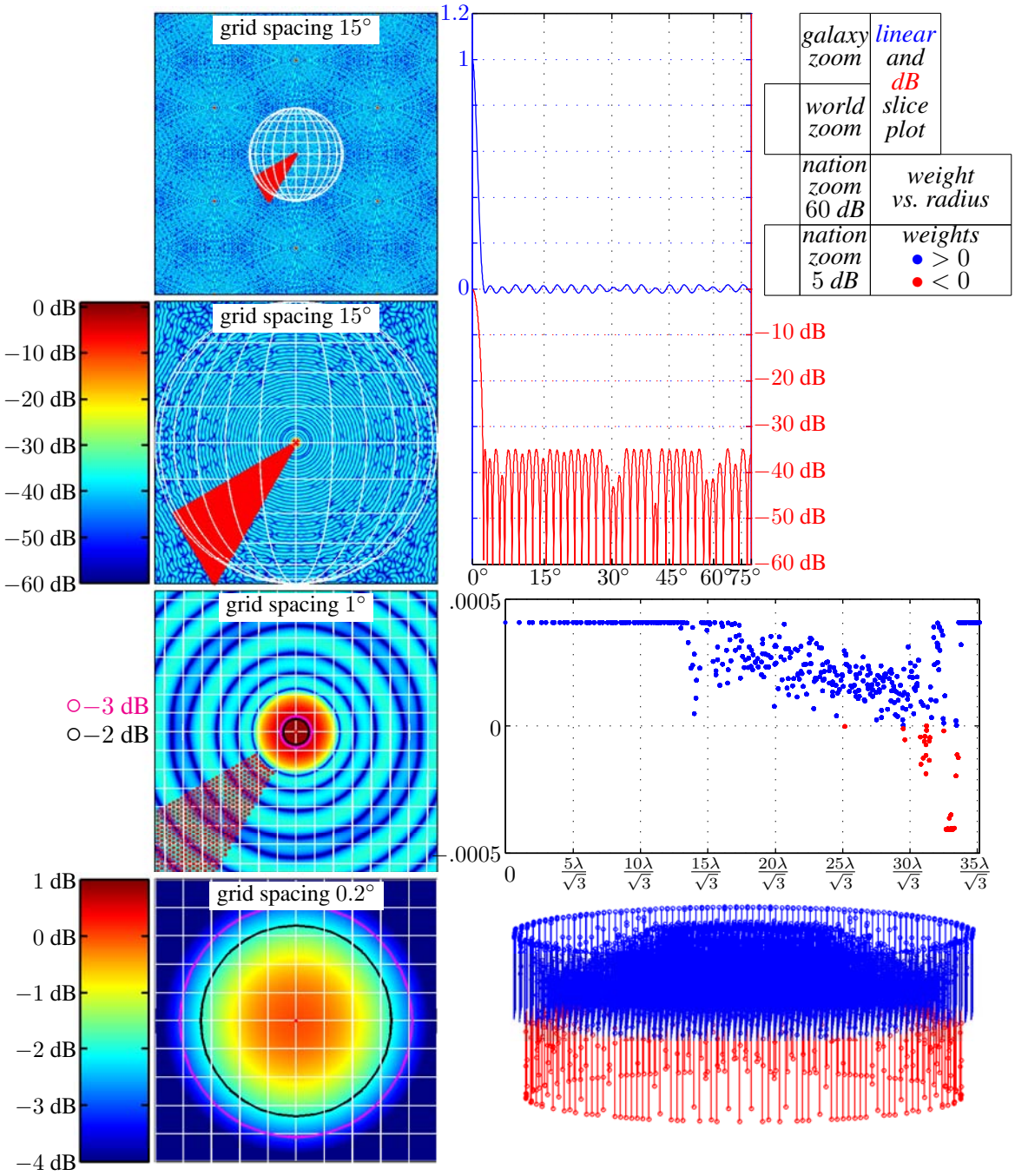

Results:

weight-energy taper loss (weight-energy taper efficiency)	2.16 dB	(60.75%)
max-weight taper loss (max-weight taper efficiency)	5.32 dB	(29.35%)
max-weight level	−67.75 dB	

Figure 15: Max-weight optimization of a Taylor-like pencil beam

Design 2.11 Max-weight optimization, mesa constraint

Next, we test the mesa constraint on our design. The mesa constraints broaden the main-beam to 4.25° to fit approximately 19 pencil beams inside the mesa (Figure 8). The following constraint is applied to the filter ($\bullet$) on the array-factor plots):

- bound the array factor between -1 dB and 0 dB in the mesa region, from boresight to 4.25°.

The average mesa loss of this case is significantly worse than the complimentary weight-energy optimization case (Design 2.4). Although the max-weight taper loss is reduced, we also have very large and undesirable sidelobes surrounding the mesa.

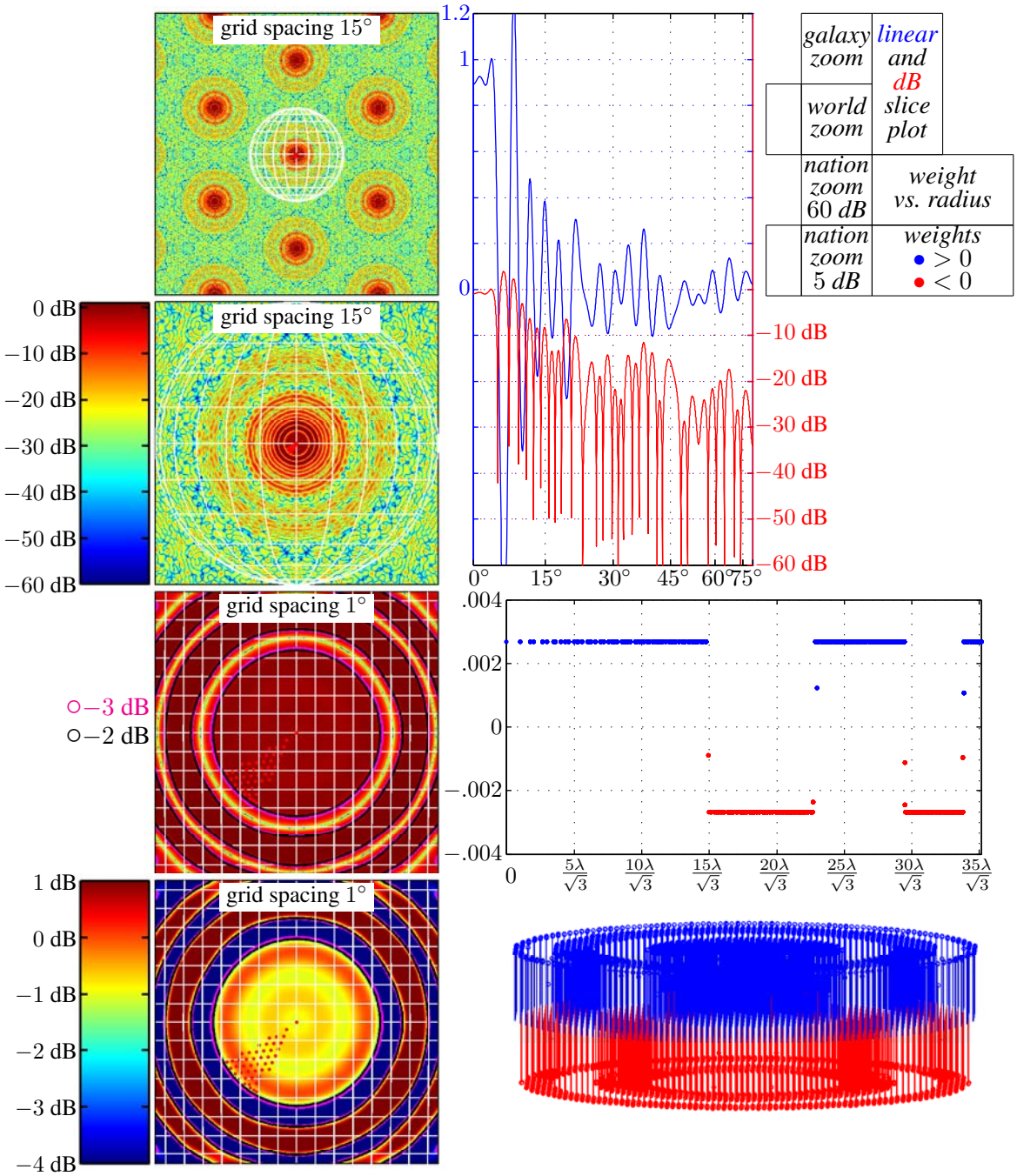

Results:

weight-energy taper loss (weight-energy taper efficiency)	22.58 dB	(0.55%)
max-weight taper loss (max-weight taper efficiency)	22.62 dB	(0.55%)
average mesa taper loss (average mesa taper efficiency)	8.07 dB	(15.58%)
max-weight level	−51.46 dB	

Figure 16: Max-weight optimization with a mesa constraint

Design 2.12 Max-weight optimization, mesa constraint, -35 dB shelf constraint

Here we combine the mesa constraint with the Taylor-like shelf constraint to get a broader beam with a Taylor-like response. The following constraints are applied to the filter (•) on the array-factor plots):

- bound the array factor between -1 dB and 0 dB in the mesa region, from boresight to $4.25°$.
- upperbound the array-factor sidelobes by -35 dB over the shelf region, from $6.8°$ outward.

Comparing this design to Design 2.5, we find the surprising result that both the weight-energy and max-weight taper losses have improved, albeit marginally. This simply reflects that here the array factor peaks up at boresight, while in Design 2.5 the array factor is depressed at boresight.

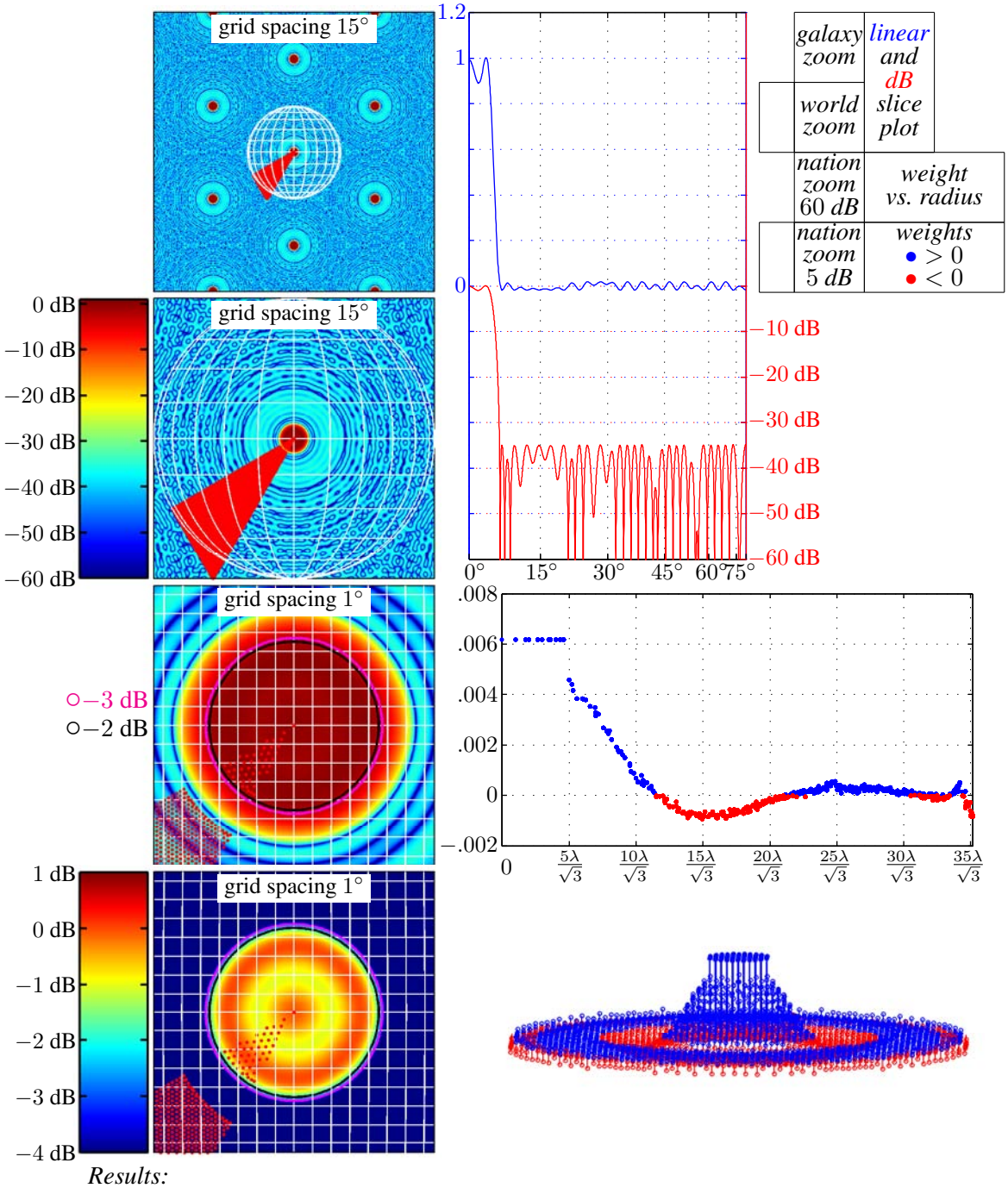

Results:

weight-energy taper loss (weight-energy taper efficiency)	14.37 dB	(3.66%)
max-weight taper loss (max-weight taper efficiency)	28.99 dB	(0.13%)
average mesa taper loss (average mesa taper efficiency)	0.13 dB	(97.05%)
max-weight level	−44.14 dB	

Figure 17: Max-weight optimization with a mesa constraint and a −35 dB Taylor-like shelf constraint

Design 2.13 Max-weight optimization, mesa constraint, -23 dB shelf constraint

Here, we change the shelf height from -35 dB, a reasonable shelf height for a Taylor-like array, to -23 dB, the target height of the brim for our sombrero designs. The following constraints are applied to the filter (•) on the array-factor plots):

- bound the array factor between -1 dB and 0 dB in the mesa region, from boresight to $4.25°$.
- upperbound the array-factor sidelobes by -23 dB over the shelf region, from $6.8°$ outward.

Here again the improvement in max-weight taper loss over Design 2.6 is minimal and accompanied by a significant loss in the average mesa taper loss.

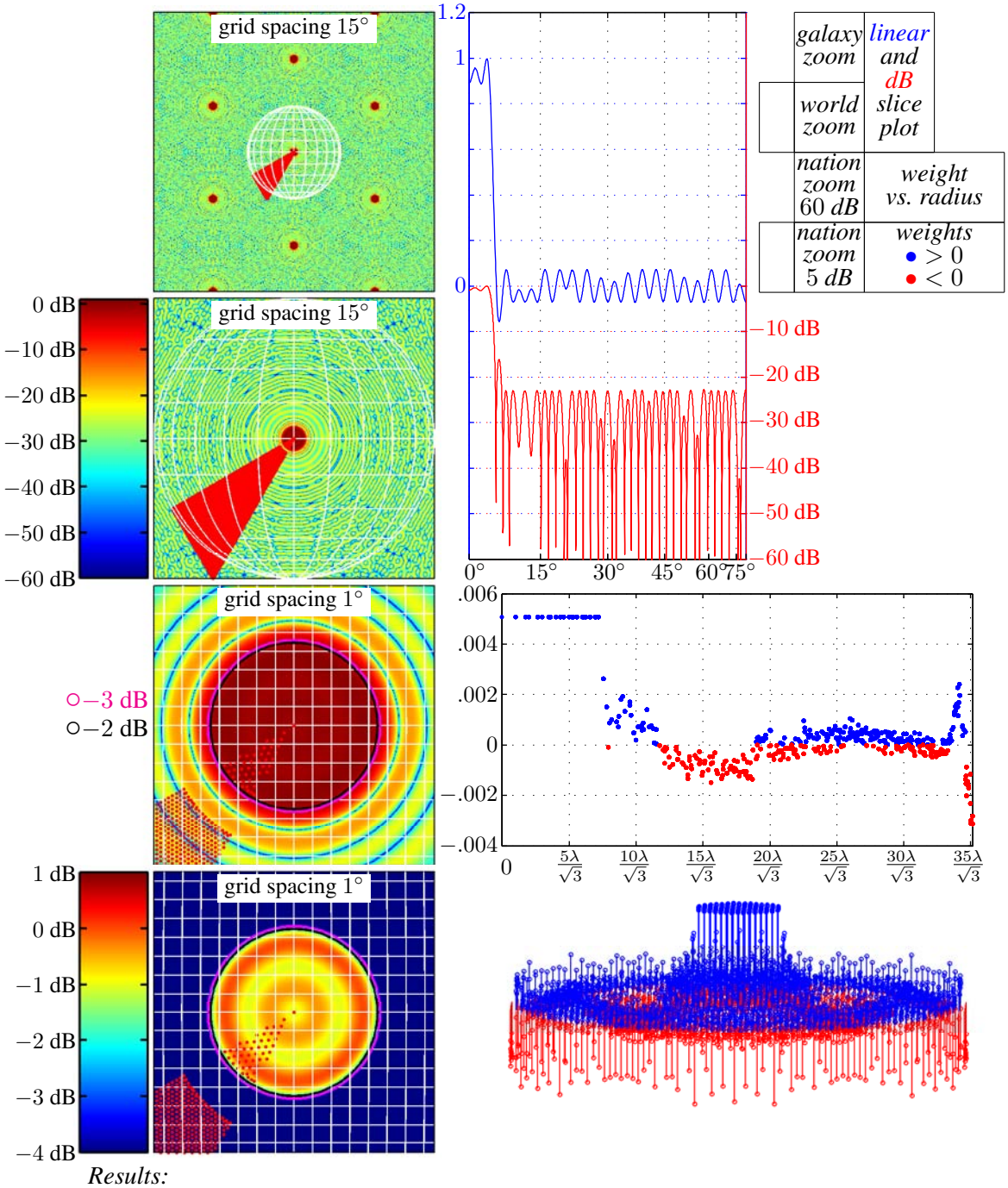

Results:

weight-energy taper loss (weight-energy taper efficiency)	16.20 dB	(2.40%)
max-weight taper loss (max-weight taper efficiency)	28.01 dB	(0.16%)
average mesa taper loss (average mesa taper efficiency)	1.26 dB	(74.76%)
max-weight level	−46.07 dB	

Figure 18: Max-weight optimization with a mesa constraint and a −23 dB Taylor-like shelf constraint

Design 2.14 Max-weight optimization, Taylor-like pencil beam, 30° brim constraint

Here we go back to a pencil-beam design (we remove the mesa constraints) and add the brim constraints (the pedestal and shelf constraints in Figure 1) to produce a sombrero-shaped array factor with a pencil-beam mesa. The following constraints are applied to the filter (•) on the array-factor plots):

- constrain the array factor at boresight to 0 dB.
- upperbound the array-factor sidelobes by -23 dB over the shelf region, from 2.5° outward (•) on the array-factor plots).
- lowerbound the array factor by -25 dB in the pedestal region, from 6.8° to 30° (○ on the array-factor plots).

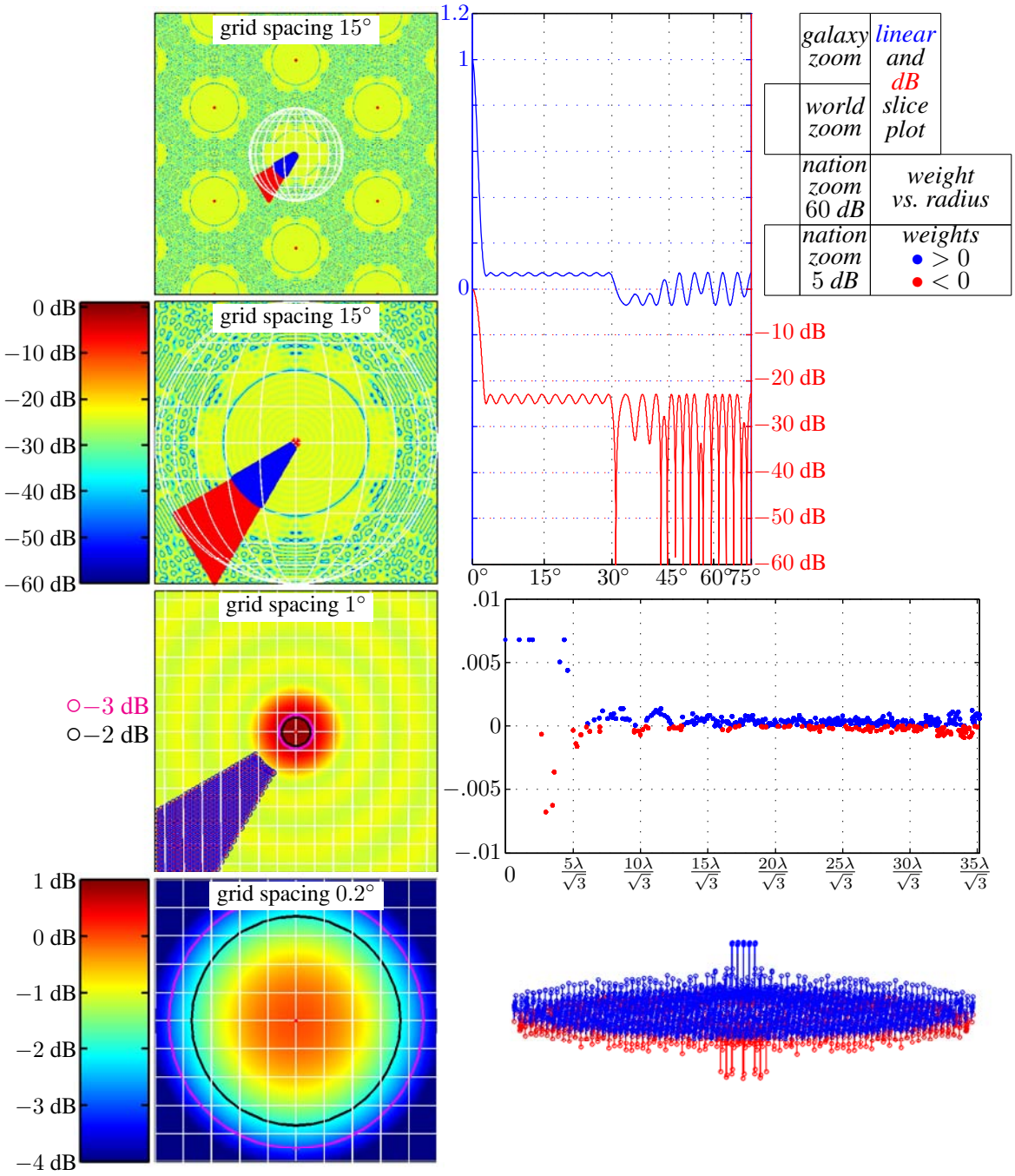

Results:

weight-energy taper loss (weight-energy taper efficiency)	11.45 dB	(7.17%)
max-weight taper loss (max-weight taper efficiency)	30.22 dB	(0.10%)
max-weight level	−42.86 dB	

Figure 19: Max-weight optimization of Taylor-like pencil beam with 30° brim constraints

Design 2.15 Max-weight optimization, sombrero constraints, 30° brim

Next, mesa constraints are reintroduced to generate our desired sombrero pattern. The constraints for the sombrero pattern are:

- bound the array factor between -1 dB and 0 dB in the mesa region, from boresight to 4.25° (•) on the array-factor plots).
- upperbound the array-factor sidelobes by -23 dB over the shelf region, from 6.8° outward (•) on the array-factor plots).
- lowerbound the array factor by -25 dB in the pedestal region, from 6.8° to 30° (○ on the array-factor plots).

The improvement in max-weight taper loss over Design 2.8 is modest.

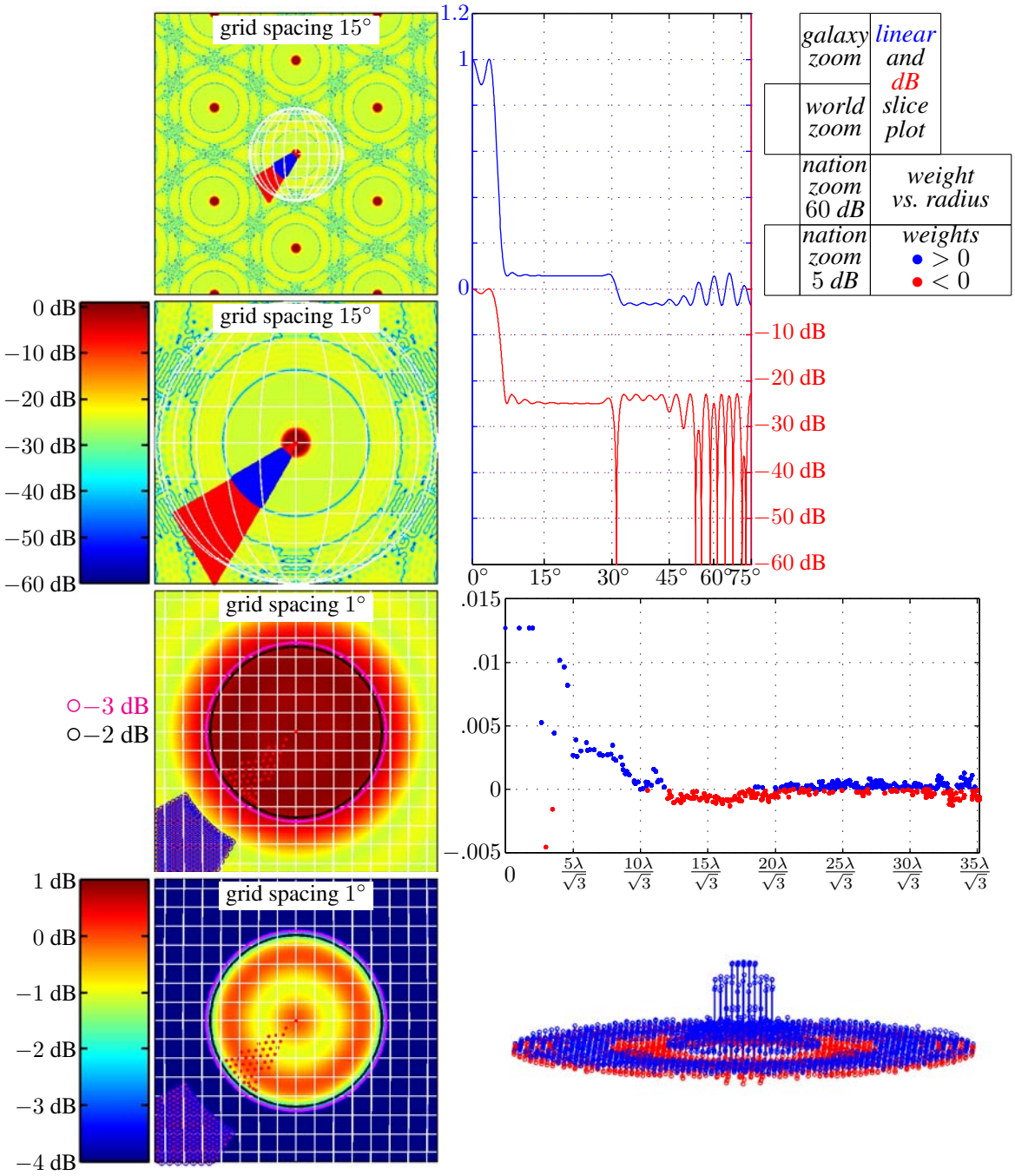

Results:

weight-energy taper loss (weight-energy taper efficiency)	16.21 dB	(2.39%)
max-weight taper loss (max-weight taper efficiency)	35.12 dB	(0.03%)
average mesa taper loss (average mesa taper efficiency)	1.96 dB	(63.70%)
max-weight level	−37.96 dB	

Figure 20: Max-weight optimization with sombrero constraints (30° brim)

Design 2.16 Max-weight optimization, sombrero constraints, 45° brim

Here is another example of the sombrero pattern, with the brim extending out to 45°. The constraints for the sombrero pattern are:

- bound the array factor between -1 dB and 0 dB in the mesa region, from boresight to 4.25° (•) on the array-factor plots).
- upperbound the array-factor sidelobes by -23 dB over the shelf region, from 6.8° outward (•) on the array-factor plots).
- lowerbound the array factor by -25 dB in the pedestal region, from 6.8° to 45° (○ on the array-factor plots).

As in many of the previous designs, compared to Design 2.9 we see a small improvement in the max-weight taper loss and similar increases in the weight-energy and average-mesa taper losses.

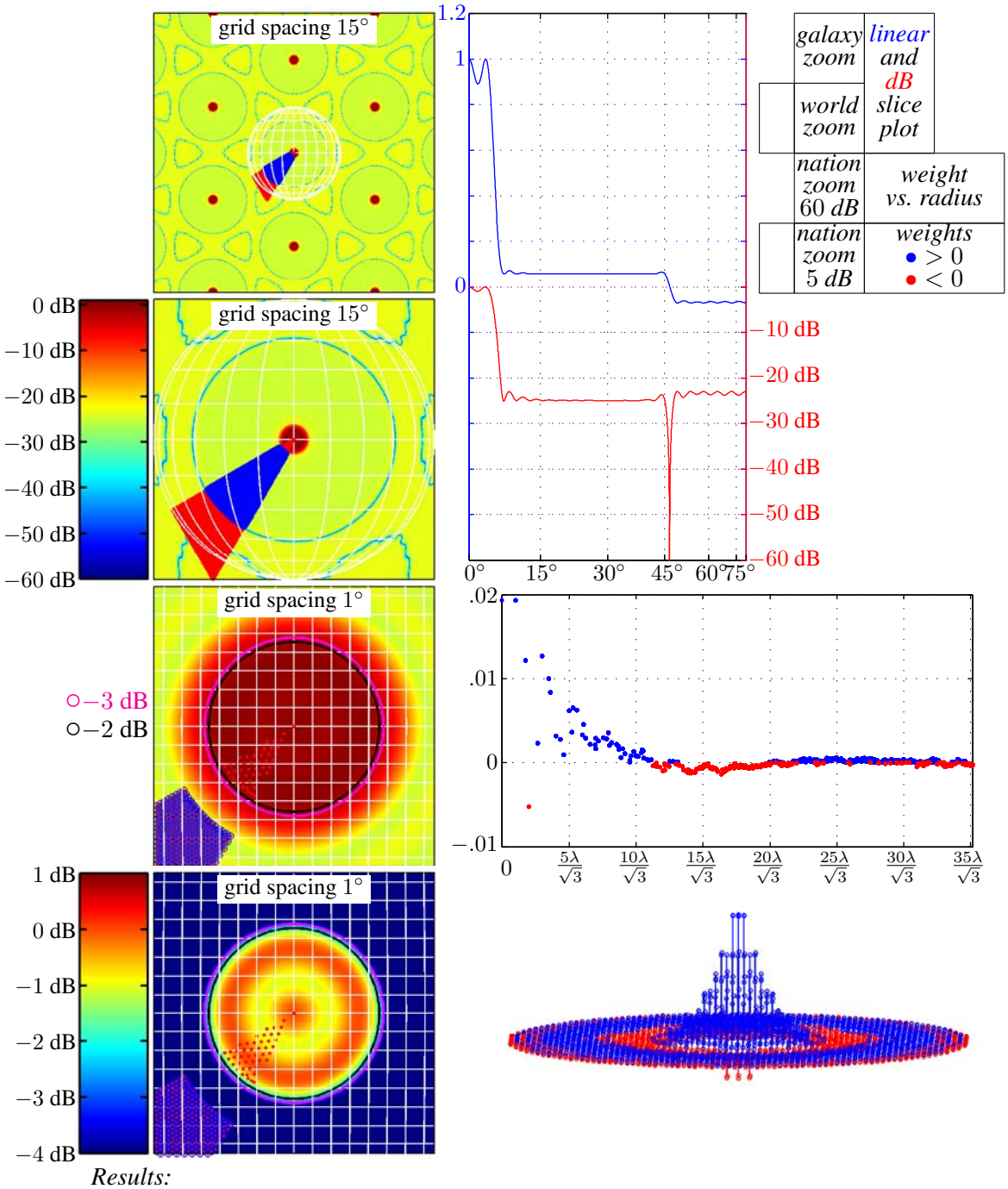

Results:

weight-energy taper loss (weight-energy taper efficiency)	16.46 dB	(2.26%)
max-weight taper loss (max-weight taper efficiency)	38.65 dB	(0.01%)
average mesa taper loss (average mesa taper efficiency)	2.20 dB	(60.29%)
max-weight level	−34.43 dB	

Figure 21: Max-weight optimization with sombrero constraints (45° brim)

3 Phase-Only Tapers

This section is based on [4] but includes both more examples and material on taper losses that is not present there.

Earlier taper designs in this report all featured real element weights. Optimization of real weights or even complex weights is practical even for large problems because the design constraints are mathematically convex: given any two tapers $u_{\mathbf{n}}$ and $v_{\mathbf{n}}$ that satisfy the constraints, any taper obtained by linearly interpolating between them, like $.7\,u_{\mathbf{n}} + .3\,v_{\mathbf{n}}$ or $.1\,u_{\mathbf{n}} + .9\,v_{\mathbf{n}}$ or $.4\,u_{\mathbf{n}} + .6\,v_{\mathbf{n}}$, satisfies those constraints as well. For such a convex optimization problem, any local optimum is also the global optimum. Further, there are efficient algorithms for finding that global optimum.

However, robust and reliable optimization of a phase-only array taper is practical only in the most limited of special cases, simply because a constant-amplitude constraint $|h_{\mathbf{n}}| = 1$ itself is nonconvex. Interpolation between two unit-magnitude complex numbers does not in general yield a unit-magnitude result; a straight line between two points on the circumference of a circle does not remain on that circumference. A large array will have several thousand of these nonconvex constraints, one per element except when elements are related by symmetry. For large arrays this typically gives the resulting optimization problem a vast, even ghastly number of local optima, and there is no reliable way of discovering which of them is the global optimum.

Viable phase-only strategies then tend to either use a heuristic method to pick a reasonable suboptimal design or to use a preliminary design chosen in that way to initialize a follow-on optimal search for a nearby local optimum. Examples of heuristic design approaches can be found in [5, 6, 7, 8, 9, 10]. Local optimization approaches are presented in [11, 12, 13, 14, 15, 16, 17]. Nonlocal optimization methods, such as simulated annealing and genetic algorithms, have also been used [18], although they do not guarantee global solutions either. There are also hybrid approaches such as [19], in which a small number of phase basis functions is heuristically chosen and the corresponding coefficients are then locally optimized. Whether any of these procedures yields a useful result depends very much on the particulars.

A simple FM-chirp heuristic approach. One heuristic approach commonly used for uniform line arrays in 1D borrows from classical FM waveform design. The core idea is simply to hope that the magnitude of a chirp's Fourier spectrum at a given frequency f is proportional to the amount of time the instantaneous frequency, given for chirp $\mathrm{e}^{\mathrm{j}\theta(t)}$ by $f_{\text{inst}}(t) = \frac{1}{2\pi}\frac{d\theta(t)}{dt}$, spends near f. It's very much like an integral change of variable $f = f_{\text{inst}}(t)$ or $t = f_{\text{inst}}^{-1}(f)$ so that $dt = \frac{df_{\text{inst}}^{-1}(f)}{df}\,df$. The chirp spends time dt between instantaneous frequencies f and $f + df$, so we might hope that its Fourier spectrum will have magnitude at least roughly proportional to $\left|\frac{df_{\text{inst}}^{-1}(f)}{df}\right|$. The messy part mathematically is generally dealing with the inverse-function aspect of this, but there are classic cases in which the relationships are not difficult to work out, and exploring them brings out the limitations of the approach.

For example, for $t \in \left(-\frac{T}{2}, \frac{T}{2}\right)$ the FM chirp waveform

$$w(t) = \begin{cases} \mathrm{e}^{\mathrm{j}\pi(\beta t)(t/T)} & \text{for } |t| < T/2, \\ 0 & \text{otherwise.} \end{cases}$$

has instantaneous frequency $\beta t/T$, which sweeps at a constant rate across interval $\left(-\frac{\beta}{2}, \frac{\beta}{2}\right)$ as t increases. One might hope then that its Fourier magnitude spectrum is roughly constant on that interval and zero elsewhere. In fact it is approximately so *when time-bandwidth product βT is large* and only then. In that case,

$$|W(f)| \approx \begin{cases} \text{some constant} & \text{for } |f| < \beta/2, \\ 0 & \text{otherwise.} \end{cases}$$

Use unsampled 2D tapers and their transforms for simplicity. We begin the extension to 2D by establishing a simplified notation. Relating that new notation to our existing notation is a tad tedious but is along the lines of the usual development of sampling in signals-and-system texts. Let the orthonormal columns of 3×2 matrix $\mathbf{A}$ point in the azimuth and elevation directions when looking out along the array boresight vector. If two-vector $\boldsymbol{x}$ contains azimuth and elevation coordinates, we can express a position in the array plane as $\mathbf{A}\boldsymbol{x}$, and we can express the array-plane component $\underline{\mathbf{k}}$ of wavenumber $\mathbf{k}$ using a two-vector $\boldsymbol{k}$ of azimuth-elevation coordinates as $\underline{\mathbf{k}} = \mathbf{A}\boldsymbol{k}$.

For simplicity let's then assume the taper is obtained by sampling a continuous function $g(\boldsymbol{x})$ at the values of $\boldsymbol{x}$ corresponding to element positions. The sampling process can be represented in the $\boldsymbol{x}$ and $\boldsymbol{k}$ domains and continuous-"time" (really space) Fourier transformation in 2D, where each sum is over all two-vectors of integers, as

$$\begin{array}{ccc} g(\boldsymbol{x}) & \overset{\text{2D CT}}{\leftrightarrow} & G(\boldsymbol{k}) \\ \times & & * \\ \lambda^2 |\mathbf{B}^{\mathrm{T}}\mathbf{B}|^{\frac{1}{2}} \sum_{\mathbf{n}} \delta(\boldsymbol{x} - \mathbf{A}^{\mathrm{T}}\lambda\mathbf{B}\mathbf{n}) & \overset{\text{2D CT}}{\leftrightarrow} & \sum_{\mathbf{m}} \delta(\boldsymbol{k} - \tfrac{1}{\lambda}(\mathbf{A}^{\mathrm{T}}\mathbf{B})^{-\mathrm{T}}\mathbf{m}) \\ || & & \\ \sum_{\mathbf{n}} \underbrace{\lambda^2 |\mathbf{B}^{\mathrm{T}}\mathbf{B}|^{\frac{1}{2}} g(\mathbf{A}^{\mathrm{T}}\lambda\mathbf{B}\mathbf{n})}_{h_{\mathbf{n}}} \delta(\boldsymbol{x} - \mathbf{A}^{\mathrm{T}}\lambda\mathbf{B}\mathbf{n}) & \overset{\text{2D CT}}{\leftrightarrow} & \underbrace{\sum_{\mathbf{n}} h_{\mathbf{n}} \, \mathrm{e}^{-\mathrm{j}2\pi \boldsymbol{k}^{\mathrm{T}}\mathbf{A}^{\mathrm{T}}\lambda\mathbf{B}\mathbf{n}}}_{H(\boldsymbol{k}^{\mathrm{T}}\mathbf{A}^{\mathrm{T}}\lambda\mathbf{B}) = H(\underline{\mathbf{k}}^{\mathrm{T}}\lambda\mathbf{B})}. \end{array}$$

The transform in the last line follows by direct evaluation of the transform integral. The underbraces identify the actual taper (left) and array factor (right) in terms of the 2D discrete-time (space) Fourier pair $h_{\mathbf{n}} \leftrightarrow H(\mathbf{f})$ used earlier for amplitude tapers. Here $g(\boldsymbol{x})$ must have units of $1/\langle\text{length}\rangle^2$ to make $h_{\mathbf{n}}$ dimensionless, and the actual array factor $H(\underline{\mathbf{k}}^{\mathrm{T}}\lambda\mathbf{B}) = H(\mathbf{k}^{\mathrm{T}}\lambda\mathbf{B})$ is then related to the $G(\boldsymbol{k})$ that we will use here by $\underline{\mathbf{k}} = \mathbf{A}\boldsymbol{k}$ and

$$H(\boldsymbol{k}^{\mathrm{T}}\mathbf{A}^{\mathrm{T}}\lambda\mathbf{B}) = \sum_{\mathbf{m}} G(\boldsymbol{k} - \tfrac{1}{\lambda}(\mathbf{A}^{\mathrm{T}}\mathbf{B})^{-\mathrm{T}}\mathbf{m}).$$

We actually have no further need of such details of scaling and periodic replication, as we derive results only up to a scale factor and assume always that the sampling-related replication amounts to little more than periodic extension.

Brick-wall beams from phase bowls. Extending the 1D chirp idea to a rectangle in array-plane coordinates is now straightforward. Beamwidth and time-extent matrices $\boldsymbol{\beta}$ and $\mathbf{T}$ are diagonal with positive elements on those diagonals:

$$g(\boldsymbol{x}) = \begin{cases} \frac{1}{\text{some area}} \, \mathrm{e}^{\mathrm{j}\pi \boldsymbol{x}^{\mathrm{T}} \boldsymbol{\beta} \mathbf{T}^{-1} \boldsymbol{x}} & \text{for } \mathbf{T}^{-1}\boldsymbol{x} \in \mathcal{S}, \\ 0 & \text{otherwise.} \end{cases} \tag{10}$$

Here set $\mathcal{S}$ is a 1×1 square centered on the origin. In 2D the instantaneous (really "instanspaceous" since $\boldsymbol{x}$ comprises position coordinates, but we lack such a word) frequency of a signal $\mathrm{e}^{\mathrm{j}\theta(\boldsymbol{x})}$ is just $\boldsymbol{k}_{\text{inst}} = \frac{1}{2\pi}\nabla\theta(\boldsymbol{x})$, with the gradient taken with respect to coordinate vector $\boldsymbol{x}$. The phase of signal $g(\boldsymbol{x})$ of (10) has the parabolic "bowl" shape $\theta(\boldsymbol{x}) = \pi \boldsymbol{x}^{\mathrm{T}} \boldsymbol{\beta} \mathbf{T}^{-1} \boldsymbol{x}$ and instantaneous frequency $\boldsymbol{k}_{\text{inst}} = \boldsymbol{\beta}\mathbf{T}^{-1}\boldsymbol{x}$, and the latter ranges across those $\boldsymbol{k}_{\text{inst}}$ for which $\boldsymbol{\beta}^{-1}\boldsymbol{k}_{\text{inst}} \in \mathcal{S}$. And indeed, when matrix $\boldsymbol{\beta}\mathbf{T}$ has large diagonal elements,

$$|G(\boldsymbol{k})| \approx \begin{cases} \text{some constant} & \text{for } \boldsymbol{\beta}^{-1}\boldsymbol{k} \in \mathcal{S}, \\ 0 & \text{otherwise.} \end{cases}$$

This continuous phase-only taper has a rectangular outline and gives an approximately rectangular beam in spatial frequency $\boldsymbol{k}$ (sine space).

For an outline elliptical in vector $\boldsymbol{x}$ we could use

$$g(\boldsymbol{x}) = \begin{cases} \frac{1}{\text{some area}} \, \mathrm{e}^{\mathrm{j}\pi \boldsymbol{x}^{\mathrm{T}} \boldsymbol{\beta} \mathbf{T}^{-1} \boldsymbol{x}} & \text{for } \boldsymbol{x}^{\mathrm{T}}\mathbf{T}^{-2}\boldsymbol{x} < \frac{1}{4}, \\ 0 & \text{otherwise,} \end{cases}$$

where 2×2 symmetric time and beamwidth matrices $\mathbf{T}$ and $\boldsymbol{\beta}$ here are positive definite. The major and minor diameters of the taper are given by the eigenvalues of $\mathbf{T}$. Again $\boldsymbol{k}_{\text{inst}} = \boldsymbol{\beta}\mathbf{T}^{-1}\boldsymbol{x}$, and in the ellipse where $g(\boldsymbol{x})$ is nonzero it ranges over the ellipse in $\boldsymbol{k}_{\text{inst}}$ for which $\boldsymbol{k}_{\text{inst}}^{\mathrm{T}}\boldsymbol{\beta}^{-2}\boldsymbol{k}_{\text{inst}} < 1/4$, so

$$|G(\boldsymbol{k})| \approx \begin{cases} \text{some constant} & \text{for } \boldsymbol{k}^{\mathrm{T}}\boldsymbol{\beta}^{-2}\boldsymbol{k} < \frac{1}{4}, \\ 0 & \text{otherwise.} \end{cases}$$

resulting in an elliptical beam with major and minor diameters given by the eigenvalues of $\boldsymbol{\beta}$. Other support regions can be used, resulting in beams with matching geometries.

Any of these continuous-space functions can be sampled spatially to obtain element weights for an array. The primary problem with such "FM beams" is that the approximation error is a function of the (eigenvalues of the) space-beamwidth product $\boldsymbol{\beta}\mathbf{T}$, which (eigenvalues) must (all) be large. Even the largest radar arrays do not have enough elements for this approximation to be reasonable—it takes hundreds of thousand elements to get down to a few dB of ripple—so we are reduced to tweaking parameters when (each eigenvalue of) $\boldsymbol{\beta}\mathbf{T}$ is rather small in hopes of "lucking into" a decent array factor.

Design examples approximating brick-wall beams. We illustrate in the design examples to follow by presenting several actual array factors. Our array and desired beam here are both circular, so the elliptical case above applies. That circularity makes both $\boldsymbol{\beta}$ and

$\mathbf{T}^{-1}$ into scaled identity matrices, so we can parameterize their product as $\alpha\mathbf{I} = \boldsymbol{\beta}\mathbf{T}^{-1}$ using a single scalar parameter α. Each of our first group of phase-only tapers therefore takes the form

$$g(\boldsymbol{x}) = \begin{cases} \frac{1}{\text{some area}}\, \mathrm{e}^{\mathrm{j}\pi\alpha\|\boldsymbol{x}\|^2} & \text{for } \|\boldsymbol{x}\| \text{ in our 4507-element array,} \\ 0 & \text{otherwise,} \end{cases} \tag{11}$$

Our spatial-extent matrix $\mathbf{T}$ is fixed by the array geometry, so choosing our one available parameter α corresponds to choosing beamwidth matrix $\boldsymbol{\beta}$. Given a desired beam size, we have no degrees of design freedom left. Here we simply pick several representative α values for the sake of illustration.

We do notice that the boresight value of the array factor seems especially sensitive to α, so given a general range for α that gives us roughly the beamwidth we seek, we generally end up fine tuning α to set this boresight value to something nonextreme.

A crude attempt at a Gaussian beam. The phase-bowl design examples just discussed have instantaneous frequencies $\boldsymbol{k}_{\text{inst}}$ that are linear in position $\boldsymbol{x}$ and so implicitly aim at having their array factors approximate "brick wall" spectra. It is no surprise therefore that nasty array-factor ripples arise as a result, and it certainly seems reasonable to attempt some sort of gradual rolloff as an alternative, in hopes that the approximations will be better, that ripple magnitudes will be significantly lower.

Towards this end, consider the taper

$$g(\boldsymbol{x}) = \begin{cases} \frac{1}{\text{some area}}\, \mathrm{e}^{\mathrm{j}2\sqrt{2\pi}\, r_0 k_0 \left(1 - \mathrm{e}^{-\left(\mathrm{erf}^{-1}(\|\boldsymbol{x}\|/r_0)\right)^2}\right)} & \text{for } \|\boldsymbol{x}\| < r_0, \\ 0 & \text{otherwise.} \end{cases} \tag{12}$$

Different authors define the error function with different scalings, but here $z = \mathrm{erf}^{-1}(y)$ refers to the odd function defined for positive arguments by

$$y = \mathrm{erf}(z) = \tfrac{2}{\sqrt{\pi}} \int_0^z \mathrm{e}^{-u^2} du.$$

A little algebra shows instantaneous frequency as a function of $\boldsymbol{x}$ to be

$$\boldsymbol{k}_{\text{inst}}(\boldsymbol{x}) = \tfrac{1}{2\pi}\nabla\text{phase}(\boldsymbol{x}) = \tfrac{1}{\|\boldsymbol{x}\|}\boldsymbol{x}\sqrt{2k_0^2}\,\mathrm{erf}^{-1}(\|\boldsymbol{x}\|/r_0),$$

and change of variable $\boldsymbol{k} = \boldsymbol{k}_{\text{inst}}(\boldsymbol{x})$ then results (shown in [4]) in the ratio of differential areas

$$\frac{d\boldsymbol{k}_{\text{inst}}^{-1}(\boldsymbol{k})}{d\boldsymbol{k}} = \frac{2r_0^2}{\pi k_0^2}\left(\frac{\frac{\sqrt{\pi}}{2}\,\mathrm{erf}\left(\|\boldsymbol{k}\|/\sqrt{2k_0^2}\right)}{\|\boldsymbol{k}\|/\sqrt{2k_0^2}}\right)\mathrm{e}^{-\|\boldsymbol{k}\|^2/(2k_0^2)}. \tag{13}$$

Then

$$|G(\boldsymbol{k})| \approx \langle\text{some constant}\rangle \times \frac{\frac{\sqrt{\pi}}{2}\,\mathrm{erf}\left(\|\boldsymbol{k}\|/\sqrt{2k_0^2}\right)}{\|\boldsymbol{k}\|/\sqrt{2k_0^2}}\,\mathrm{e}^{-\|\boldsymbol{k}\|^2/(2k_0^2)}, \tag{14}$$

at least for sufficiently high $r_0 k_0$, which here serves the role of a time-bandwidth product. The quantity in large parenthesis in (13) goes to unity as $\boldsymbol{k}$ goes to zero, and the error

function approaches $\sqrt{2/\pi}$ for large arguments, so the Fourier spectrum approximated in (14) is essentially Gaussian for $\|\boldsymbol{k}\| \ll k_0$ but rolls off somewhat faster than Gaussian for $\|\boldsymbol{k}\| \gg k_0$.

We present designs below for $r_0 = 20.31\lambda$, and several different values of k_0. It is no surprise that the array factor approximates the value here more closely when $r_0 k_0$ is large and that for beam sizes of interest $r_0 k_0$ in fact is fairly small. Still the resulting array-factor ripple magnitudes can sometimes be made far lower than for the phase-bowl tapers by choosing r_0 and k_0 carefully. Generally approximation quality is far more sensitive to k_0 than to r_0, and again the value of the array factor at boresight, at the origin, is particularly sensitive. Very small deviations from the k_0 values shown can triple or quadruple mainbeam ripple.

Sombrero-shaped array factor. One possible way to generate a sombrero-shaped phase-only array taper is to replace $\|\boldsymbol{x}\|$ in (12) with some function $f(\|\boldsymbol{x}\|)$ giving

$$g(\boldsymbol{x}) = \begin{cases} \frac{1}{\text{some area}} \, \mathrm{e}^{\,\mathrm{j}2\sqrt{2\pi}\, r_0 k_0 \left(1 - \mathrm{e}^{-\left(\left(\mathrm{erf}^{-1}(f(\|\boldsymbol{x}\|)/r_0)\right)^2\right)}\right)} & \text{for } \|\boldsymbol{x}\| < r_0, \\ 0 & \text{otherwise.} \end{cases} \tag{15}$$

We present several designs below using $f(\|\boldsymbol{x}\|) = b\|\boldsymbol{x}\| + (a^m + \|\boldsymbol{x}\|^m)^{1/m} - a$. As with the previous phase-only designs, small deviations in any one of the five parameters k_0, r_0, a, b, or m cause major changes in the array factor.

Presentation of individual designs. For each phase-only design that follows, the array-factor magnitudes are shown normalized to a maximum magnitude of 0 dB. Array-factor phases are nonzero but are not shown. The phase of the element weights are plotted in 3D in the lower right. The plot above that represents instantaneous frequency along an arbitrary cut through the array origin with $\boldsymbol{k}_{\text{inst}}$ equal to the plotted quantity times a unit vector in the cut direction. The average mesa taper loss of (6) (page 10) is calculated using $\underline{\phi}$ of (7) (page 10) with a mesa radius parameter k_r customized to that specific design by searching for a minimum in the spirit of Figure 5 (page 11).

Design 3.1 Linear-FM chirp, small α

Here we use LFM chirp (11) with a small α. The 3 dB beamwidth of this design is similar to the beamwidth of our amplitude-taper pencil-beam designs (Design 2.3 and Design 2.10), but the rolloff in this design is much slower.

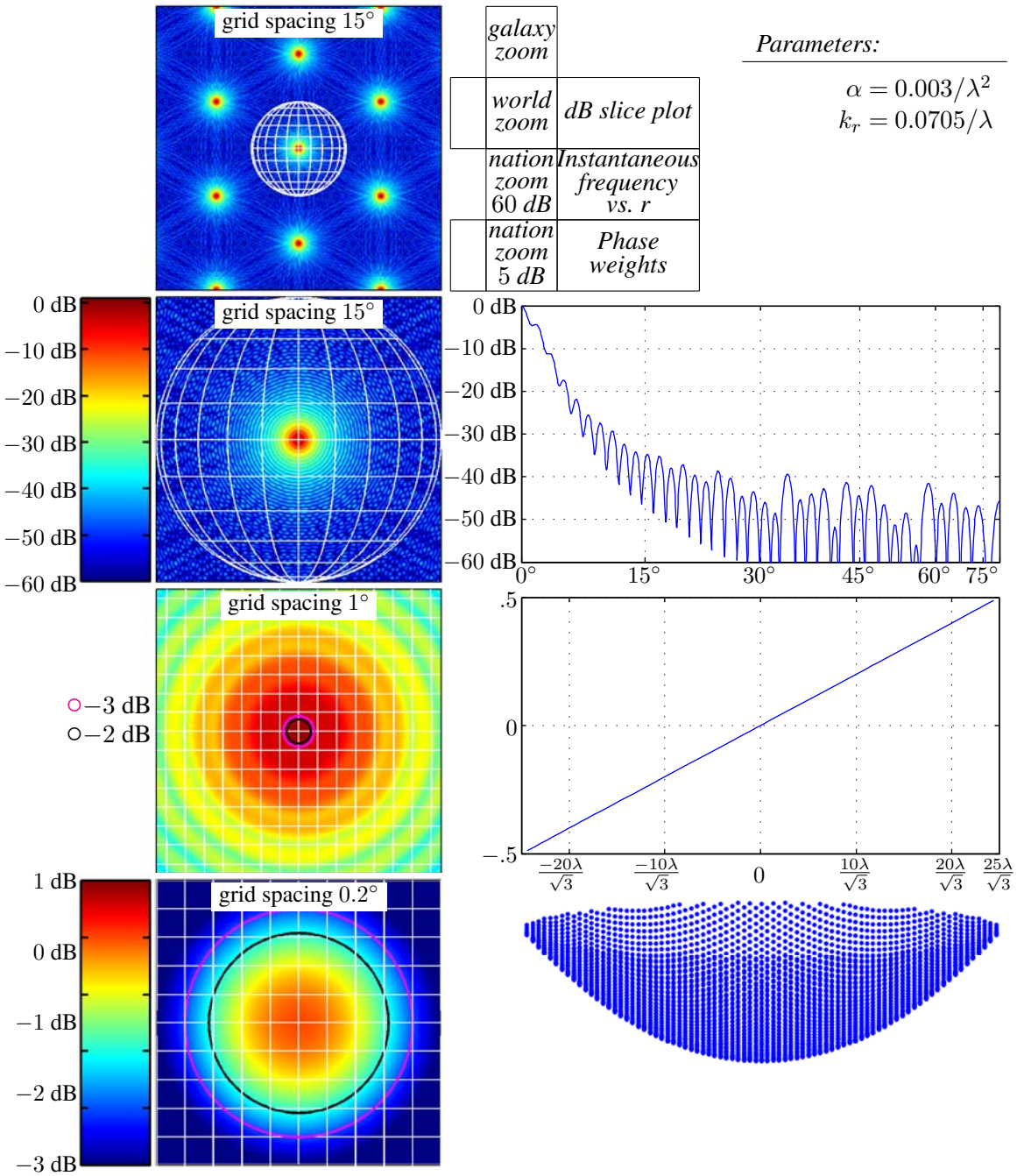

Results:

weight-energy taper loss (weight-energy taper efficiency)	6.45 dB	(22.64%)
max-weight taper loss (max-weight taper efficiency)	6.45 dB	(22.64%)
average mesa taper loss (average mesa taper efficiency)	1.11 dB	(77.36%)

Figure 22: Linear-FM chirp, small α

Design 3.2 Linear-FM chirp, medium α

Here we use LFM chirp (11) with a medium α. The 3 dB beamwidth of this design is similar to the beamwidth of our amplitude-taper mesa constrained designs (Design 2.4 and Design 2.11). Compared to those mesa constrained designs, the ripple in this design is predictably bad, the rolloff is much slower and the overall sidelobe level is higher. However, we do see a significant improvement in the max-weight taper loss when compared to our optimized amplitude-taper designs.

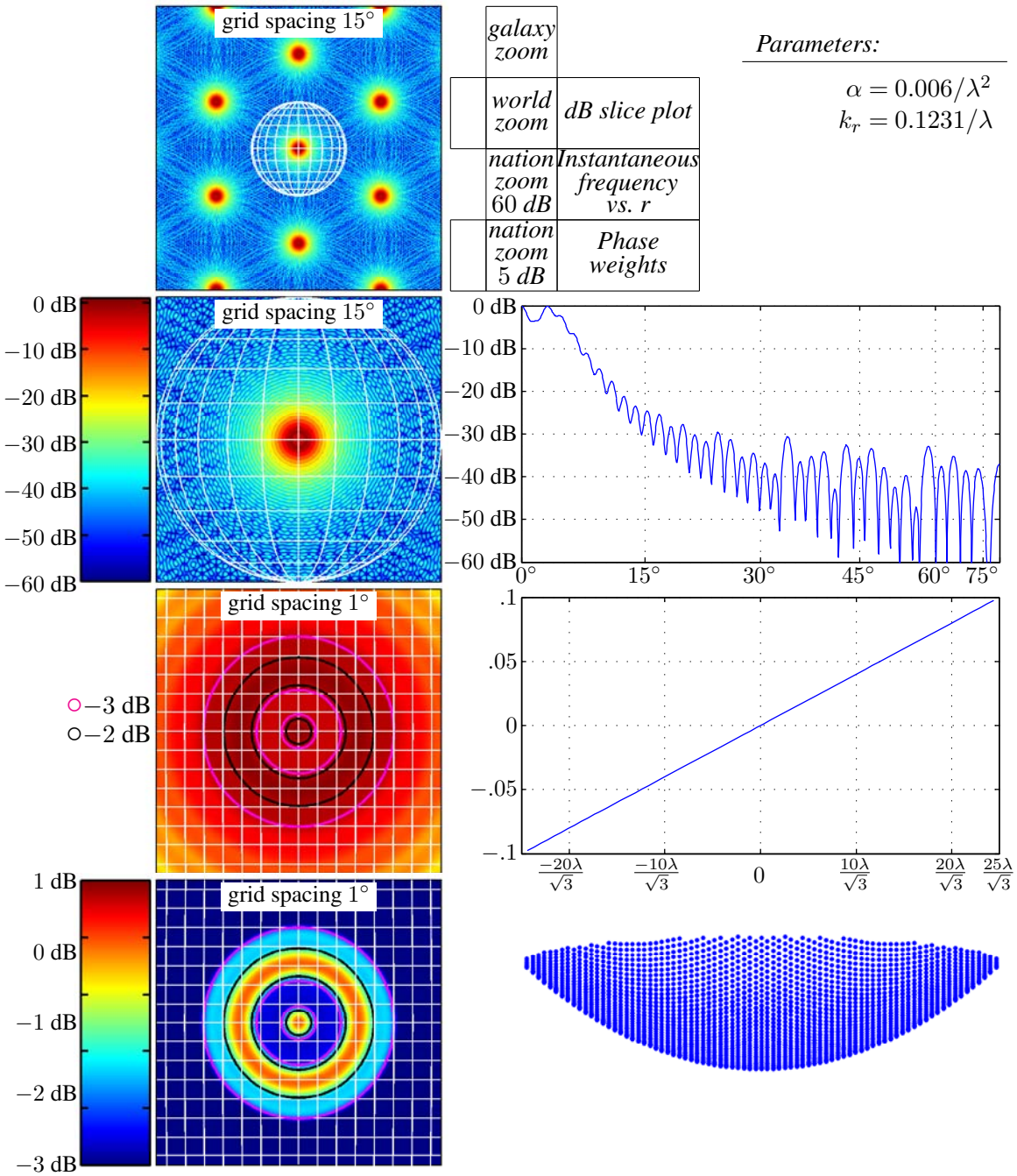

Results:

weight-energy taper loss (weight-energy taper efficiency)	15.04 dB	(3.13%)
max-weight taper loss (max-weight taper efficiency)	15.04 dB	(3.13%)
average mesa taper loss (average mesa taper efficiency)	0.84 dB	(82.45%)

Figure 23: Linear-FM chirp, medium α

Design 3.3 Linear-FM chirp, large α

Here we use LFM chirp (11) with a large α, which gives us a design with a larger mesa. Both the ripple in the mesa and the difference in the boresight array factor are very sensitive to α.

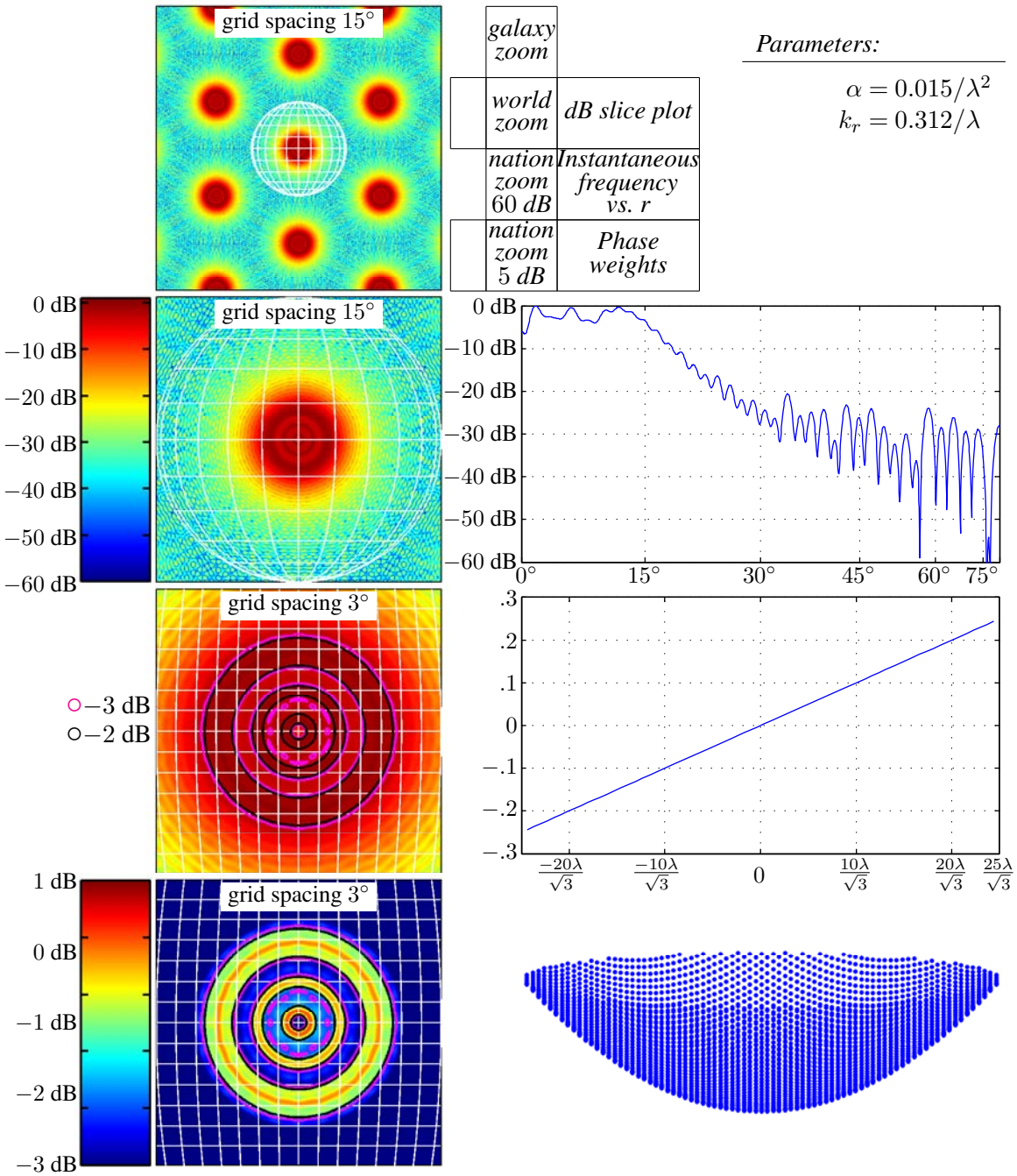

Results:

weight-energy taper loss (weight-energy taper efficiency)	29.46 dB	(0.11%)
max-weight taper loss (max-weight taper efficiency)	29.46 dB	(0.11%)
average mesa taper loss (average mesa taper efficiency)	0.58 dB	(87.59%)

Figure 24: Linear-FM chirp, large α

Design 3.4 Nonlinear-FM chirp for narrow Gaussian beam

Here we use (12) with a fixed r_0 and a small k_0.

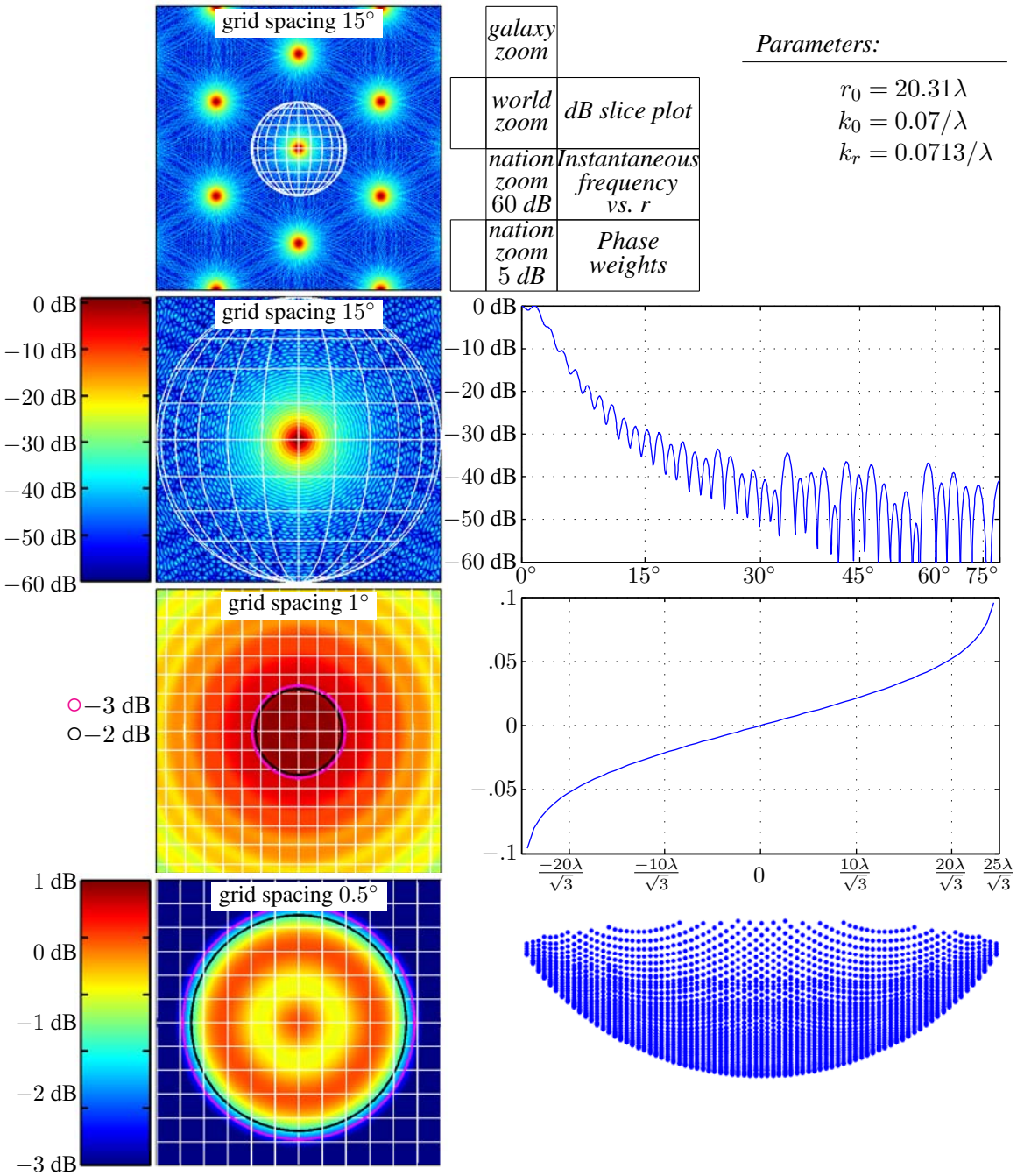

Results:

weight-energy taper loss (weight-energy taper efficiency)	11.15 dB	(7.68%)
max-weight taper loss (max-weight taper efficiency)	11.15 dB	(7.68%)
average mesa taper loss (average mesa taper efficiency)	1.25 dB	(74.98%)

Figure 25: Nonlinear-FM chirp for Gaussian beam, small k_0

Design 3.5 Nonlinear-FM chirp for medium-width Gaussian beam

Here we use (12) with a fixed r_0 and a medium k_0. This design is comparable to Design 3.2 and our amplitude-taper mesa designs (Design 2.4 and Design 2.11). Compared to Design 2.4 the weight-energy and average-mesa taper losses are both somewhat worse, and as expected the max-weight taper loss is significantly improved. Compared to Design 2.11 all the taper losses are significantly improved. The ripple in the mesa is much smaller in this design than in Design 3.2 and the roll-off and sidelobe levels are similar.

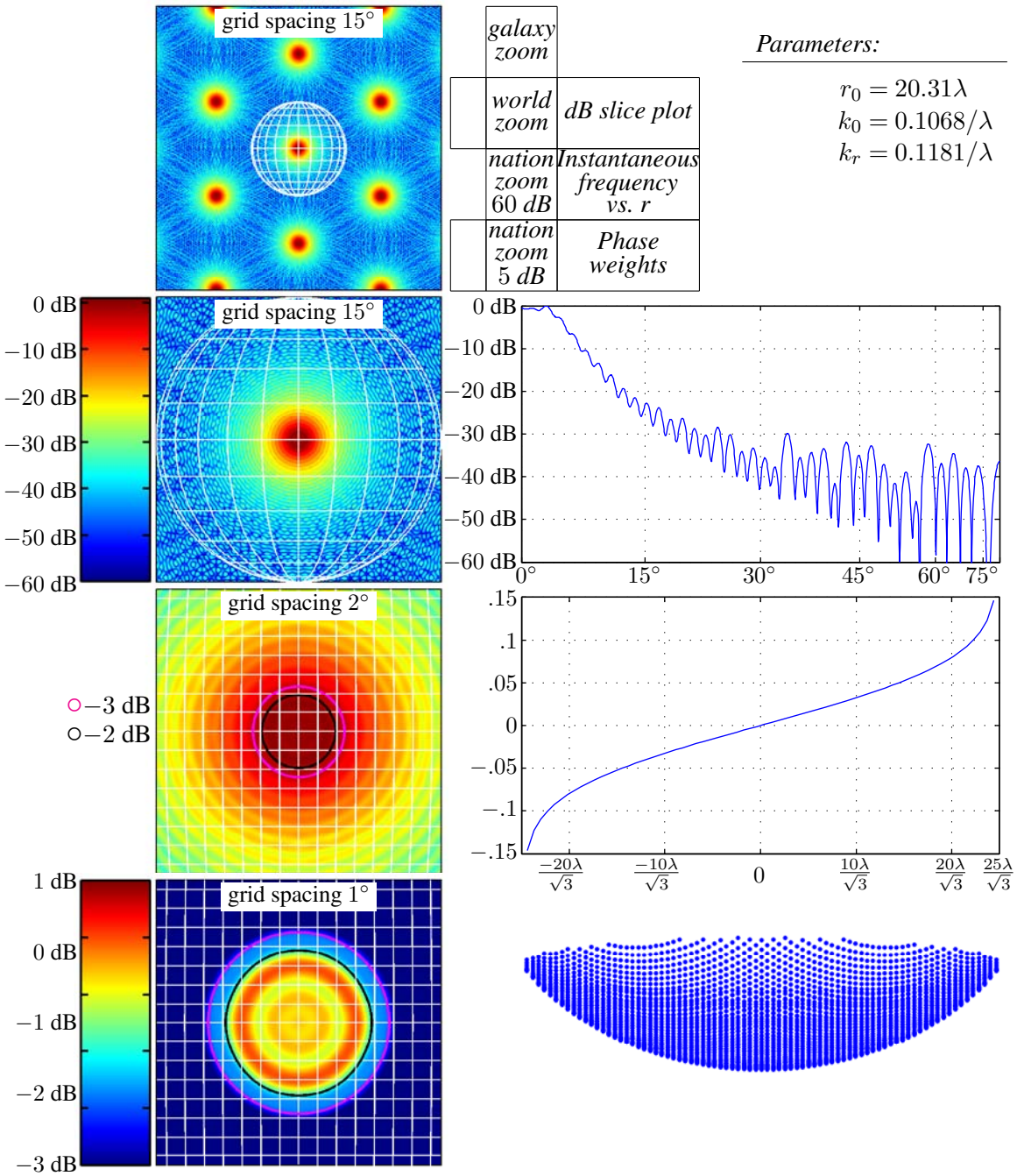

Results:

weight-energy taper loss (weight-energy taper efficiency)	16.04 dB	(2.49%)
max-weight taper loss (max-weight taper efficiency)	16.04 dB	(2.49%)
average mesa taper loss (average mesa taper efficiency)	1.07 dB	(78.14%)

Figure 26: Nonlinear-FM chirp for Gaussian beam, medium k_0

Design 3.6 Nonlinear-FM chirp for wide Gaussian beam

Here we use (12) with a fixed r_0 and a large k_0. These parameters generate a design with a larger mesa comparable to Design 3.3. The ripple in the mesa is much smaller in this design than in Design 3.3, but the roll-off and sidelobe levels are not as good.

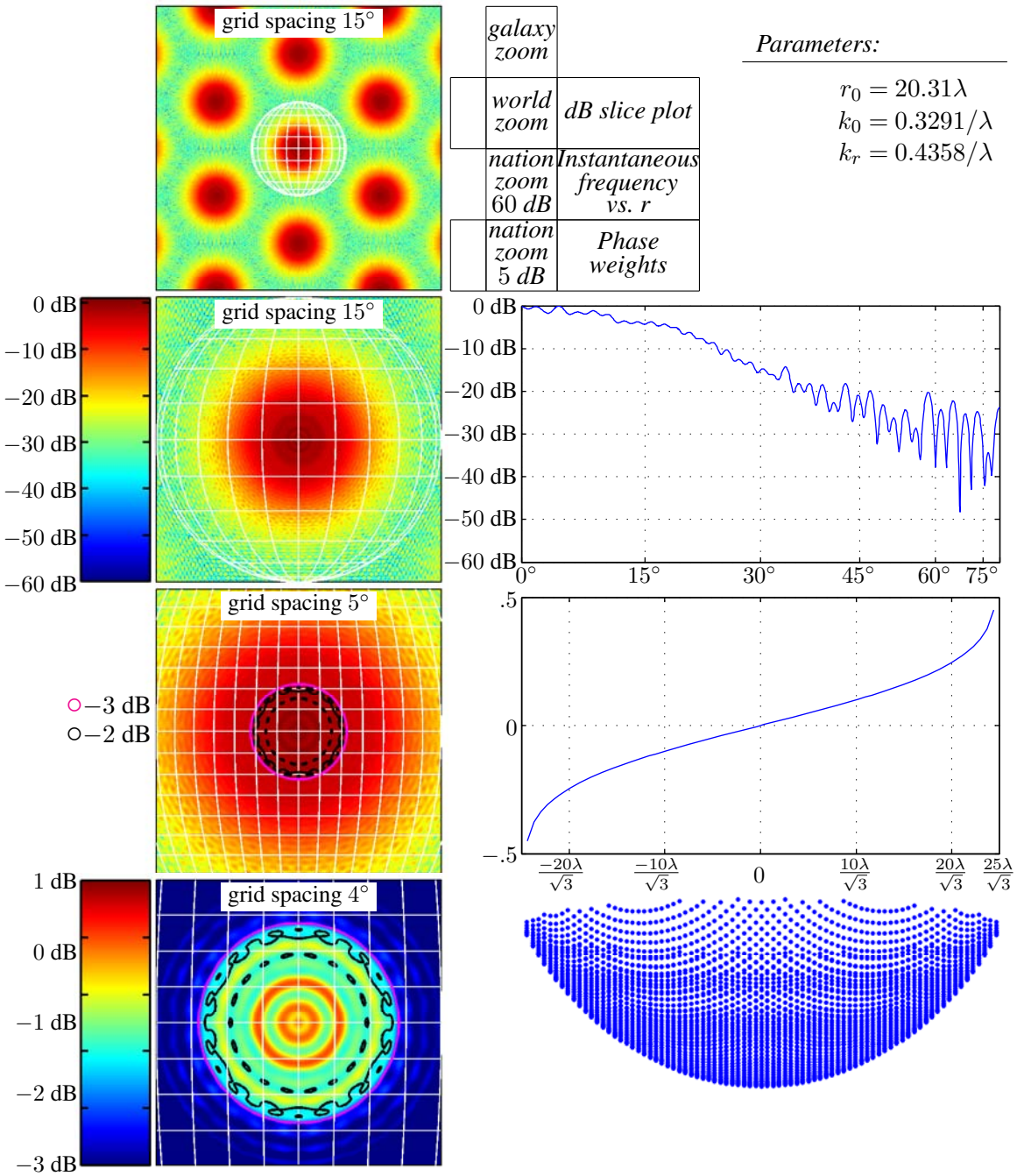

Results:

weight-energy taper loss (weight-energy taper efficiency)	24.94 dB	(0.32%)
max-weight taper loss (max-weight taper efficiency)	24.94 dB	(0.32%)
average mesa taper loss (average mesa taper efficiency)	0.84 dB	(82.46%)

Figure 27: Nonlinear-FM chirp for Gaussian beam, large k_0

Design 3.7 Nonlinear-FM chirp for sombrero beam, first try

Here we use (15). For this design, the mesa is flat for approximately $2.5°$, there is a -15 dB shelf to approximately $30°$ and a sidelobe level of -30 dB at $90°$.

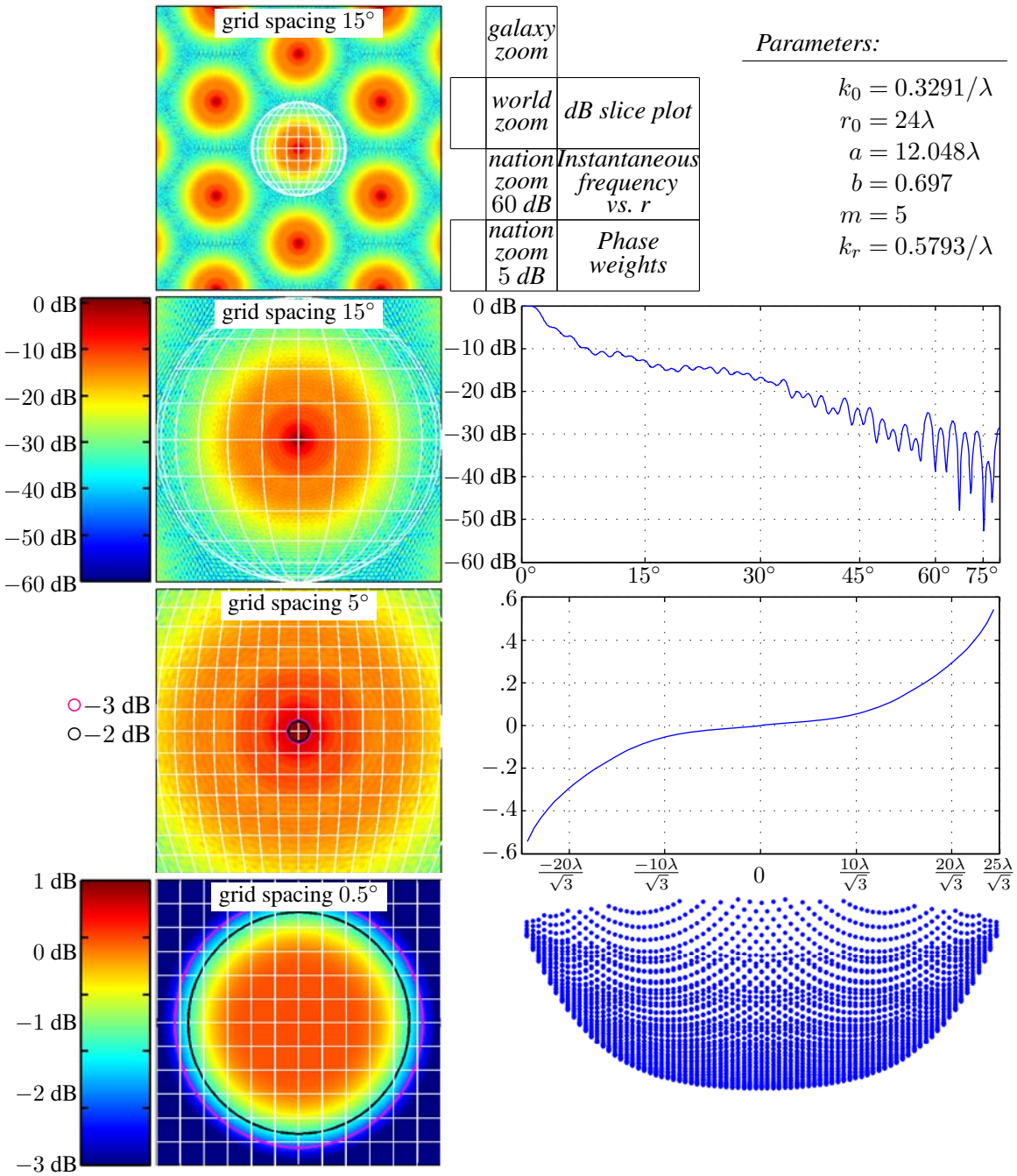

Results:

weight-energy taper loss (weight-energy taper efficiency)	18.26 dB	(1.49%)
max-weight taper loss (max-weight taper efficiency)	18.26 dB	(1.49%)
average mesa taper loss (average mesa taper efficiency)	1.32 dB	(73.85%)

Figure 28: Nonlinear-FM chirp for sombrero beam, first try

Design 3.8 Nonlinear-FM chirp for sombrero beam, better transition

Here is another design using (15).

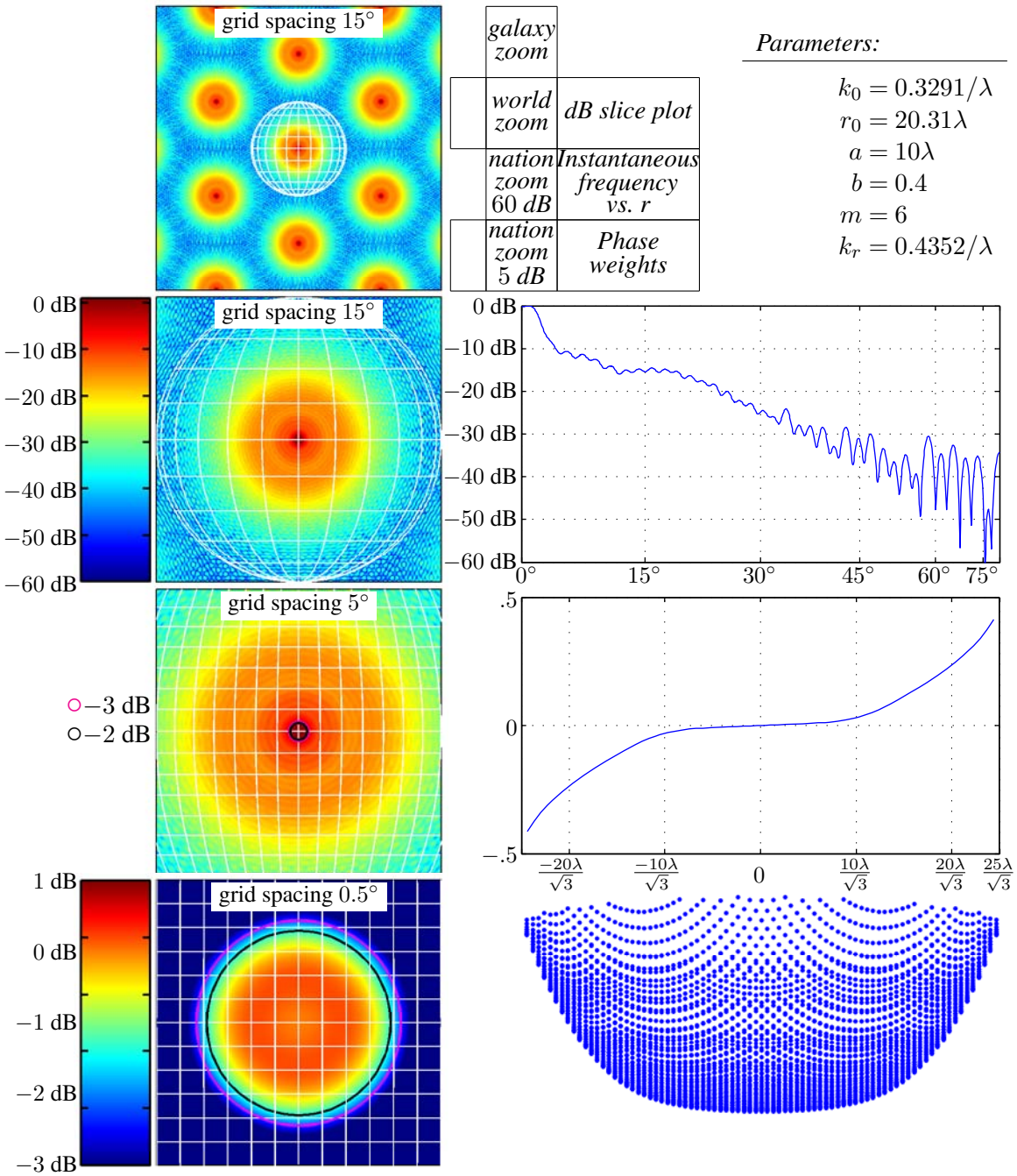

Results:

weight-energy taper loss (weight-energy taper efficiency)	15.32 dB	(2.94%)
max-weight taper loss (max-weight taper efficiency)	15.32 dB	(2.94%)
average mesa taper loss (average mesa taper efficiency)	1.37 dB	(72.95%)

Figure 29: Nonlinear-FM chirp for sombrero beam, better transition

Design 3.9 Nonlinear-FM chirp for sombrero beam, pointy beam

Here we use (15). This design has a pointy beamed mesa with a slow transition to a shelf and rolloff comparable to Design 3.7.

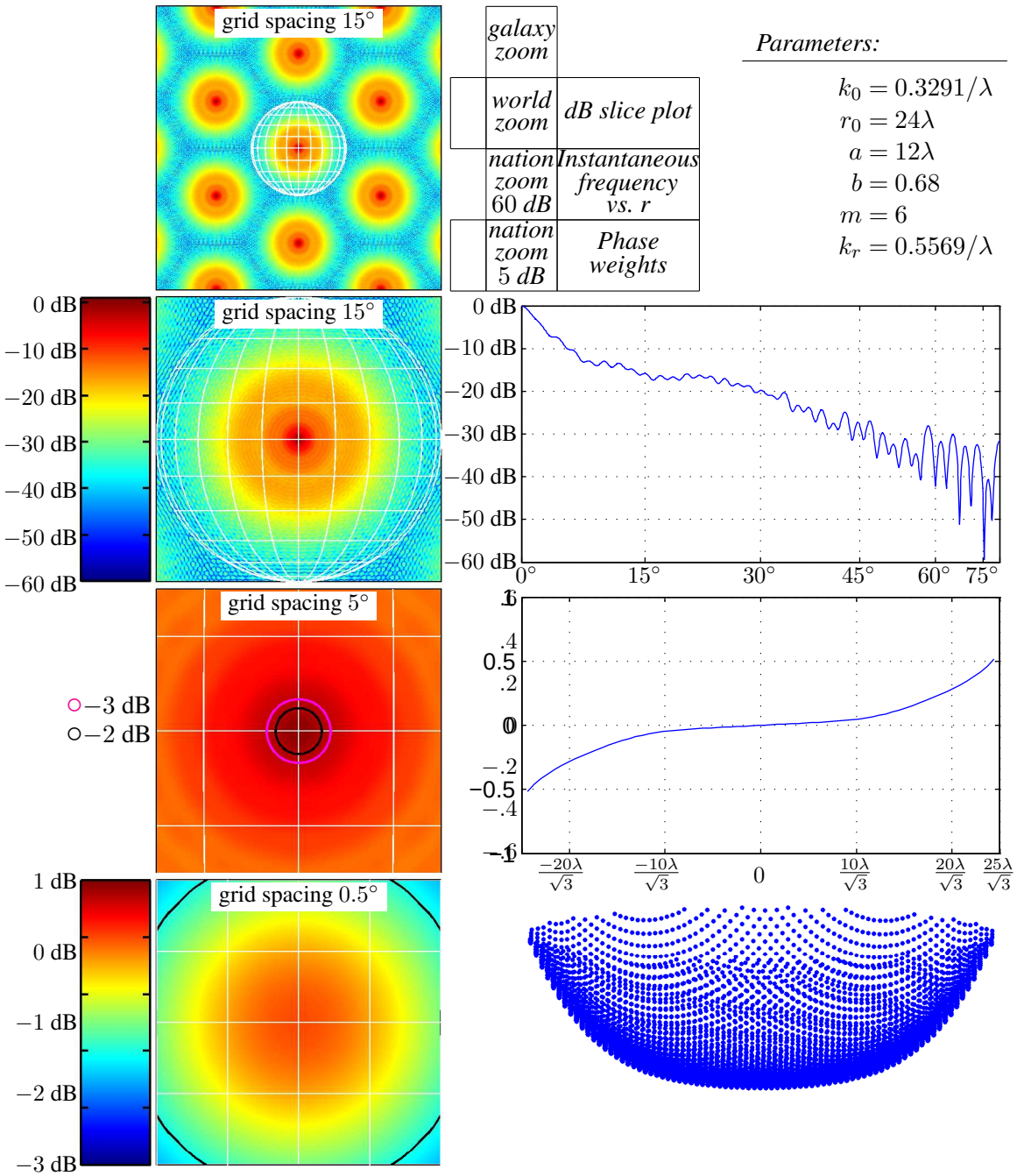

Results:

weight-energy taper loss (weight-energy taper efficiency)	15.78 dB	(2.64%)
max-weight taper loss (max-weight taper efficiency)	15.78 dB	(2.64%)
average mesa taper loss (average mesa taper efficiency)	1.35 dB	(73.36%)

Figure 30: Nonlinear-FM chirp for sombrero beam, pointy beam

4 Conclusions

Optimizing sombrero-shaped amplitude (or complex) tapers is, although not a trivial problem, one that we can successfully solve with our current optimization tools. Of the two amplitude-taper optimization objectives presented, minimizing total transmitter power while (approximately) fixing boresight or mesa-averaged radiated power density generally produces better results than minimizing the maximum element power. For the most part the latter simply increases the weight-energy and average mesa taper losses without bringing the max-weight taper loss anywhere near a reasonable number and at the additional cost of irregular and sometimes large sidelobes. There may be specific situations where some gentle constraints on the peak element weights would be useful, but in general if the array to be designed is heavily peak limited then an amplitude taper appears to be a rather poor choice. Unfortunately, current digital-array driver concepts are inherently peak limited.

Phase-only tapers do, when designs comparable to optimized amplitude tapers are discovered, significantly improve the taper loss in the peak-limited element case. However, we cannot generate a sombrero shaped phase-only design with the same degree of control and performance as an amplitude taper when the same array geometry is used. The phase-only sombrero shaped designs shown here were generated by tweaking five different parameters in (15). Each of these five parameters has significant effects on the array factor, but those effects are not systematic. The designs were a result of guessing a starting point and hand adjusting the parameters to attempt to design a reasonable sombrero shaped array factor. This process could be formalized by directly optimizing such parameters or even the phases themselves, but the presence of large numbers of local minima would make it impractically expensive to exhaustively search for the global minimum.

Design	Optimization variable	level	weight-energy taper loss	max-weight taper loss	average mesa taper loss
Uniform	N/A	N/A	0 dB	0 dB	N/A
Taylor Pencil	weight energy	−35.71 dB	0.83 dB	6.25 dB	N/A
Mesa	weight energy	−22.55 dB	14.99 dB	29.97 dB	0.02 dB
Taylor Mesa −35 dB	weight energy	−22.43 dB	15.11 dB	30.98 dB	0.06 dB
Taylor Mesa −23 dB	weight energy	−22.54 dB	15.00 dB	30.20 dB	0.02 dB
Taylor Brim	weight energy	−28.41 dB	8.13 dB	37.01 dB	N/A
Sombrero 30°	weight energy	−21.68 dB	15.86 dB	40.55 dB	0.75 dB
Sombrero 45°	weight energy	−21.22 dB	16.32 dB	44.77 dB	1.20 dB
Taylor Pencil	max weight	−67.75 dB	2.16 dB	5.32 dB	N/A
Mesa	max weight	−51.46 dB	22.58 dB	22.62 dB	8.07 dB
Taylor Mesa −35 dB	max weight	−44.14 dB	14.37 dB	28.99 dB	0.13 dB
Taylor Mesa −23 dB	max weight	−46.07 dB	16.20 dB	28.01 dB	1.26 dB
Taylor Brim	max weight	−42.86 dB	11.45 dB	30.22 dB	N/A
Sombrero 30°	max weight	−37.96 dB	16.21 dB	35.12 dB	1.96 dB
Sombrero 45°	max weight	−34.43 dB	16.46 dB	38.65 dB	2.20 dB

Table 1: Amplitude-taper results

Design	variable	weight-energy taper loss	max-weight taper loss	average mesa taper loss
Linear-FM chirp	$\alpha = 0.003/\lambda^2$	6.45 dB	6.45 dB	1.11 dB
Linear-FM chirp	$\alpha = 0.006/\lambda^2$	15.04 dB	15.04 dB	0.84 dB
Linear-FM chirp	$\alpha = 0.015/\lambda^2$	29.46 dB	29.46 dB	0.58 dB
Nonlinear-FM chirp Gaussian beam	$k_0 = 0.07/\lambda$	11.15 dB	11.15 dB	1.25 dB
Nonlinear-FM chirp Gaussian beam	$k_0 = 0.1068/\lambda$	16.04 dB	16.04 dB	1.07 dB
Nonlinear-FM chirp Gaussian beam	$k_0 = 0.3291/\lambda$	24.94 dB	24.94 dB	0.84 dB
Nonlinear-FM chirp Sombrero beam	$k_0 = 0.3291/\lambda$ $r_0 = 24\lambda$ $a = 12.048\lambda$ $b = 0.697$ $m = 5$	18.26 dB	18.26 dB	1.32 dB
Nonlinear-FM chirp Sombrero beam	$k_0 = 0.3291/\lambda$ $r_0 = 20.31\lambda$ $a = 10\lambda$ $b = 0.4$ $m = 6$	15.32 dB	15.32 dB	1.37 dB
Nonlinear-FM chirp Sombrero beam	$k_0 = 0.3291/\lambda$ $r_0 = 24\lambda$ $a = 12\lambda$ $b = 0.68$ $m = 6$	15.78 dB	15.78 dB	1.35 dB

Table 2: Phase-only taper results

References

[1] M. Skolnik, "Systems aspects of digital beamforming ubiquitous radar," Naval Research Laboratory, NRL Memo Report 8625, 28 June 2002.

[2] J. J. Alter, J. L. Block, C. E. Fox, J. A. Pavco, R. M. White, F. F. Kretschmer, I. D. Olin, and C. L. Temes, "Ubiquitous radar: A concept study," Naval Research Laboratory, NRL Memo Report 10069, 23 Nov 2004.

[3] J. O. Coleman, D. P. Scholnik, and J. J. Brandriss, "A specification language for the optimal design of exotic FIR filters with second-order cone programs," in *IEEE Asilomar Conf. on Signals, Systems, and Computers*, Pacific Grove CA, USA, Nov. 2002, pp. 341–345.

[4] J. O. Coleman, D. P. Scholnik, and K. R. McPhail, "Phase-only tapers for regular planar arrays, a heuristic nonlinear-FM approach," in *IEEE Int'l Symp. Phased Array Systems & Technology*, Oct. 2010, submitted.

[5] P. Sridevi, G. Raju, and P. Misra, "Effect of digital phase shifters on phase only controlled SLS difference patterns," in *Electromagnetic Interference and Compatibility '97. Proceedings of the International Conference on*, 1997, pp. 163–166.

[6] R. Kinsey, "Phased array beam spoiling technique," in *Antennas and Propagation Society International Symposium, 1997. IEEE., 1997 Digest*, vol. 2, 1997, pp. 698–701 vol.2.

[7] R. Young, "Antenna pattern control by phase-only weighting," in *Phased Arrays, IEE Colloquium on*, 1991, pp. 5/1–5/7.

[8] H. Steyskal, "Simple method for pattern nulling by phase perturbation," *Antennas and Propagation, IEEE Transactions on*, vol. 31, no. 1, pp. 163–166, 1983.

[9] A. Chakraborty, B. Das, and G. Sanyal, "Beam shaping using nonlinear phase distribution in a uniformly spaced array," *Antennas and Propagation, IEEE Transactions on*, vol. 30, no. 5, pp. 1031–1034, 1982.

[10] A. S. Dunbar, "On the theory of antenna beam shaping," *Journal of Applied Physics*, vol. 23, no. 8, pp. 847–853, 1952. [Online]. Available: http://link.aip.org/link/?JAP/23/847/1

[11] J. C. Kerce, G. Brown, and M. Mitchell, "Phase-Only transmit beam broadening for improved radar search performance," in *Radar Conference, 2007 IEEE*, 2007, pp. 451–456.

[12] S. Sun and H. Li, "Simplified beamforming on phase-only arrays," in *Neural Networks and Signal Processing, 2003. Proceedings of the 2003 International Conference on*, vol. 2, 2003, pp. 1290–1293 Vol.2.

[13] A. Khzmalyan and A. Kondratiev, "The phase-only shaping and adaptive nulling of an amplitude pattern," *Antennas and Propagation, IEEE Transactions on*, vol. 51, no. 2, pp. 264–272, 2003.

[14] O. Bucci, G. D'Etia, and G. Romito, "Optimal synthesis of reconfigurable conformal arrays with phase only control," in *Antennas and Propagation Society International Symposium, 1996. AP-S. Digest*, vol. 2, 1996, pp. 810–813 vol.2.

[15] D. Chang, C. Hung, C. Hu, K. Ho, and H. Chen, "Synthesis of array antenna with broad nulls," in *Microwave Conference Proceedings, 1993. APMC '93., 1993 Asia-Pacific*, vol. 1, 1993, pp. 1–88–1–92 vol.1.

[16] E. Dufort, "Pattern synthesis based on adaptive array theory," *Antennas and Propagation, IEEE Transactions on*, vol. 37, no. 8, pp. 1011–1018, 1989.

[17] R. Voges and J. Butler, "Phase optimization of antenna array gain with constrained amplitude excitation," *Antennas and Propagation, IEEE Transactions on*, vol. 20, no. 4, pp. 432–436, 1972.

[18] A. Trastoy, F. Ares, and E. Moreno, "Phase-only control of antenna sum and shaped patterns through null perturbation," *Antennas and Propagation Magazine, IEEE*, vol. 43, no. 6, pp. 45–54, 2001.

[19] L. Marcaccioli, R. V. Gatti, and R. Sorrentino, "Series expansion method for phase-only shaped beam synthesis and adaptive nulling," *URSI EMTS*, 2004.